eLife

Reviewed Preprint
v1 • June 2, 2026
Not revised

For correspondence:
carlaliaci@gmail.com
Giorgia.Quadrato@med.usc.edu
giorgioroberto.merlo@unito.it

Competing interests: No competing interests declared

Funding: See page 27

Reviewing editor: Nicolás Unsain, Universidad Nacional de Córdoba, Argentina

© 2026, Liaci et al. This article is distributed under the terms of the Creative Commons Attribution License, which permits unrestricted use and redistribution provided that the original author and source are credited.

ARHGEF6-dependent cytoskeletal regulation underlies a conserved program of forebrain interneuron development

Carla Liaci[1,2,3], Beatrice Savarese[1,4,5], Elena Ferretti[1], Jean-Paul Urenda[2,3], Junyu Joanna Lu[2,3], Giovanni Catapano[1], Lucia Prandi[1,6], Mattia Camera[1,7], Rohin Manohar[2,3], Simona Rando[1,8], Alessandro Umbach[9], Enis Hidisoglu[10,11], Giuseppe Chiantia[5], Andrea Marcantoni[10], Maurizio Giustetto[5], Roberto Oleari[12], Alyssa Paganoni[12], Anna Cariboni[12], Van Truong[2,3], Luciano Conti[9], Giorgia Quadrato[2,3], Giorgio R Merlo[1]

[1]Department of Molecular Biotechnologies and Health Sciences, University of Turin, Turin, Italy • [2]Department of Stem Cell Biology and Regenerative Medicine, Keck School of Medicine, University of Southern California, Los Angeles, United States • [3]Eli and Edythe Broad CIRM Center for Regenerative Medicine and Stem Cell Research at USC, Keck School of Medicine, University of Southern California, Los Angeles, United States • [4]Rita Levi-Montalcini Department of Neuroscience, University of Turin, Turin, Italy • [5]Neuroscience Institute Cavalieri Ottolenghi University of Turin, Orbassano, Italy • [6]Human Technopole, Milan, Italy • [7]Department of Neuroscience, Rehabilitation, Ophthalmology, Genetics and Maternal and Child Sciences (DINOGMI), University of Genoa, Genoa, Italy • [8]Department of Clinical and Biological Sciences, University of Turin, Turin, Italy • [9]Department of Cellular, Computational and Integrative Biology (CIBIO), University of Trento, Trento, Italy • [10]Department of Drug Science, NIS Center, University of Turin, Turin, Italy • [11]Faculty of Medicine, Department of Biophysics, Izmir Bakircay University, Izmir, Turkiye • [12]Department of Pharmacological and Biomolecular Sciences, University of Milan, Milan, Italy

eLife Assessment

The study presents **valuable** findings regarding the impact of ARHGEF6 deletion, a RhoGTPase regulator linked to X-linked intellectual disability (XLID46), in the development of interneurons. The evidence supporting the observed cellular and developmental phenotypes collected in both mouse and human iPSC models is **convincing**, although further work would strengthen the mechanistic interpretation and clarify the specificity of the findings. This work offers new insights into ARHGEF6 function and the potential contribution of its dysfunction to neurodevelopmental disorders.

https://doi.org/10.7554/eLife.111288.1.sa4

Abstract

The molecular programs coordinating inhibitory interneuron migration, maturation, and survival during forebrain development remain incompletely understood. Here we investigate ARHGEF6, a RAC1/CDC42 guanine nucleotide exchange factor linked to X-linked intellectual disability (XLID46) and previously studied only at postsynaptic compartments, and reveal an earlier, conserved role in forebrain interneuron development. ARHGEF6 is selectively enriched in the inhibitory lineage during the peak of interneuron generation and migration. Its loss in mice reduces the number of cortical and hippocampal interneurons, disrupts tangential migration, increases developmental cell death, and impairs morphological and electrophysiological maturation. Strikingly, *ARHGEF6*-knockout human iPSC-derived organoids and assembloids mirror these deficits exhibiting increased apoptosis, reduced neuronal output, disorganized growth cones, impaired neurite branching, and disrupted migratory dynamics. These cross-species findings reframe ARHGEF6 as

an early, essential orchestrator of inhibitory circuit assembly and reveal a conserved cytoskeletal program whose disruption produces the excitatory-inhibitory imbalance linked to cognitive dysfunction.

Introduction

The assembly of functional forebrain circuits depends on the precise coordination of three linked processes during development: the directed migration of newborn neurons to their target destinations, the elaboration of their dendritic and axonal arbors, and their survival through developmental checkpoints governed by activity and connectivity (Southwell et al., 2012; Heck et al., 2008; Wong et al., 2018; Causeret et al., 2018; Wong & Marín, 2019). All three processes require dynamic remodeling of the actin cytoskeleton, and all three are disproportionately sensitive to disruption in GABAergic interneurons (INs), which must travel extraordinary distances from their birthplace in the ventral telencephalon to populate the developing cortex and hippocampus (Marín & Rubenstein, 2001; Wonders & Anderson, 2006; Marín, 2013). Despite representing only a minority of the total neuronal population, cortical and hippocampal INs regulate virtually all aspects of local circuit maturation and activity through their morphological, neurochemical, and functional diversity (Pelkey et al., 2017; Lim et al., 2018).

The Rho family of small GTPases, including RHOA, RAC1, and CDC42, are the principal molecular switches that couple extracellular guidance signals to cytoskeletal rearrangements during cell migration and morphogenesis. They cycle between an inactive GDP-bound state and an active GTP-bound state under tight control by guanine nucleotide exchange factors (GEFs), which promote activation, GTPase-activating proteins (GAPs), which stimulate GTP hydrolysis and inactivation, and guanine nucleotide dissociation inhibitors (GDIs), which stabilize the inactive GDP-bound state and prevent reactivation. In neurons, this regulatory network controls axon extension and guidance, growth cone formation and rearrangement, dendritic arborization, and the structural and functional plasticity of synapses (Govek et al., 2011; Tejada-Simon, 2015; Martino et al., 2013; Liaci et al., 2021). Importantly, RAC1 and its regulators play early roles in telencephalic progenitors, influencing self-renewal and cell fate decisions, including the transition of inhibitory progenitors from G1 to S phase via cyclin D and Rb phosphorylation (Vidaki et al., 2012; Lian et al., 2019; Hass et al., 2025). Notably, hundreds of genes have been associated with intellectual disability (ID) (Gupta, 2023; Maia et al., 2021), many of which, including *PAK3*, *ARHGEF6*, *ARHGEF7*, *ARHGEF9*, *OPHN1*, *TRIO*, and *FGD1*, encode regulators and effectors of the Rho family of small GTPases (Liaci et al., 2021).

ARHGEF6 (α-PIX/cool-2) is a guanine nucleotide exchange factor for RAC1 and CDC42 that is well-positioned to coordinate this cytoskeletal program. It contains a tandem Dbl homology (DH)–pleckstrin homology (PH) domain pair conferring catalytic GEF activity, an SH3 domain that recruits p21-activated kinases PAK1–3, and it associates with the ARF GAP scaffold proteins GIT1 and GIT2, placing ARHGEF6 at the intersection of RAC1/CDC42 and ARF GTPase signaling (Manser et al., 1998; Zhou et al., 2016). In the mouse hippocampus, ARHGEF6 localizes within dendritic spines and colocalizes with the postsynaptic marker PSD95, consistent with association with postsynaptic density complexes; its loss or depletion alters spine morphology and density, as well as synaptic plasticity, including reduced long-term potentiation and enhanced long-term depression at the Schaffer collateral–CA1 synapse (Nodé-Langlois et al., 2006; Ramakers et al., 2012). ARHGEF6 has also been proposed to participate in Reelin-dependent Golgi positioning during apical dendrite selection (Meseke et al., 2013). These studies established a postsynaptic role for ARHGEF6 in hippocampal pyramidal neurons, but its function during earlier stages of forebrain development, and specifically in the inhibitory lineage, had not been explored.

Variants in ARHGEF6 have been proposed as the genetic basis for X-linked intellectual disability type 46 (XLID46/MRX46; OMIM 300436), initially identified through a reciprocal X;21 translocation and a segregating intronic variant in a large Dutch pedigree (Kutsche et al., 2000; Yntema et al., 1998). However, subsequent population-level re-evaluation found the reported intronic variant at appreciable frequency in hemizygous males, and clinical curation efforts have accordingly

questioned the strength of evidence for a direct causal relationship (Genomics England PanelApp; Piton et al., 2013). This genetic uncertainty is not unusual for rare X-linked conditions, where definitive human genetic evidence may remain elusive for years. What has been missing is direct functional evidence in human neurons. Crucially, the broader RAC1 regulatory network is robustly implicated in neurodevelopmental disorders: variants in RAC1 itself cause a syndrome with intellectual disability, cortical malformations, and developmental delay (Reijnders et al., 2017; Banka et al., 2022), reinforcing the notion that disruption of this signaling axis has major developmental consequences in the human brain.

Here, we show that *ARHGEF6* expression is enriched in the GABAergic inhibitory lineage of the developing mouse and human telencephalon, revealing a developmental pattern distinct from its previously described postsynaptic role. We demonstrate that ARHGEF6 is required for the tangential migration, morphological maturation, electrophysiological development, and survival of forebrain INs in the mouse, and that these requirements are conserved in human ventral forebrain organoids and dorsal–ventral assembloids derived from *ARHGEF6*-knockout (KO) human induced pluripotent stem cells. Together, our findings identify ARHGEF6 as a conserved regulator of IN development and provide a cellular framework for how its disruption may impair inhibitory circuit formation and contribute to cognitive dysfunction. More broadly, this study highlights the value of cross-species models for defining developmental mechanisms relevant to neurodevelopmental disease.

Results

1. Developmental and cell type-specific expression of *ARHGEF6* in the telencephalon

To initially investigate the potential developmental impact of *ARHGEF6* in the human brain, particularly in light of its implication in the pathoetiology of ID, we analyzed publicly available transcriptomic datasets. Bulk RNA-sequencing data from human fetal brain samples at post-conception weeks (PCW) 8–9 revealed *ARHGEF6* is expressed across multiple brain regions (Allen Human Brain Atlas: BrainSpan, Atlas of the Developing Brain; *RRID:SCR_008083*); Fig. 1A). Expression levels were relatively elevated in ventral telencephalic regions, including the ganglionic eminences (GEs), particularly the medial (MGE) and caudal (CGE) ganglionic eminences (Fig. 1A), which serve as the principal sources of cortical GABAergic INs during early neurodevelopment. This developmental stage is characterized by intense proliferative activity within the GEs, the onset of IN production, and the early phases of their tangential migration toward the developing cortex (Hansen et al., 2013; Paredes et al., 2016; Keefe et al., 2023). Elevated expression was also observed in the upper rhombic lip (URL) and in the amygdala (AMY), consistent with the developmental origin of several of its nuclei, such as the central and medial amygdala, which are comprised of GE-derived progenitor domains that predominantly generate GABAergic neurons (Aerts et al., 2021; Prakash et al., 2025).

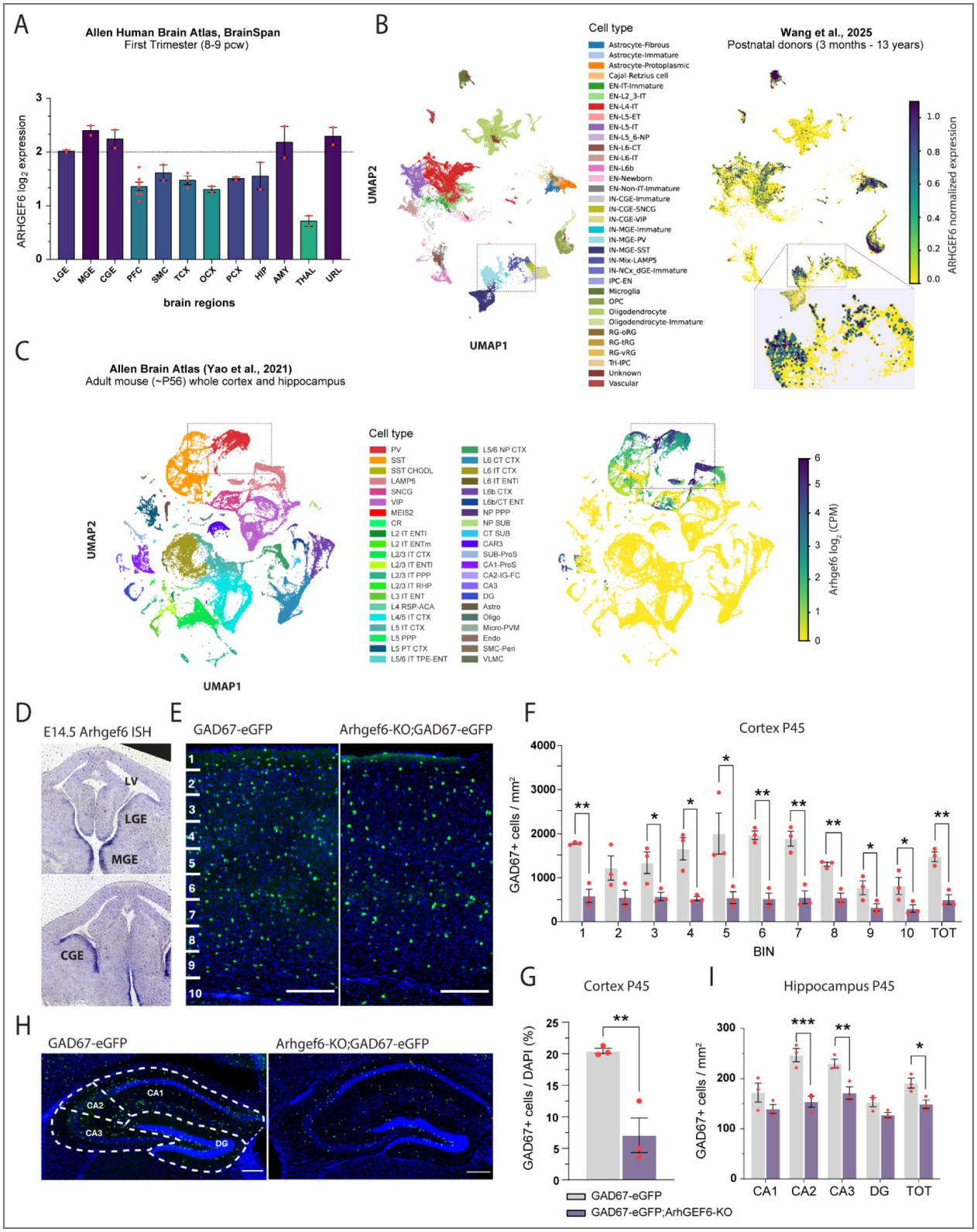

Figure 1. *ARHGEF6* expression in the ventral telencephalic lineage and reduced GABAergic IN number in the *Arhgef6-KO* murine telencephalon.

A. *ARHGEF6* expression across brain regions between 8-9 post-conception weeks from bulk RNA-seq data. 30 total samples from 2 unique donors. The dashed line indicates the minimum level of expression detected in the ganglionic eminences (GEs). PFC, prefrontal cortex (areas: dorsolateral prefrontal cortex, anterior [rostral] cingulate [medial

prefrontal] cortex, orbital frontal cortex, ventrolateral prefrontal cortex); SMC, sensorimotor cortex (areas: primary motor cortex [area M1, area 4], primary somatosensory cortex [area S1, areas 3, 1, 2], primary motor-sensory cortex); TCX, temporal cortex (areas: temporal neocortex, posterior [caudal] superior temporal cortex, inferolateral temporal cortex [area TEv, area 20], primary auditory cortex [core]); OCX, occipital cortex (areas: occipital neocortex, primary visual cortex [striate cortex, area V1/17]); PCX, parietal cortex (areas: parietal neocortex, posteroventral [inferior] parietal cortex); HIP, hippocampus (areas: hippocampus [hippocampal formation]); AMY, amygdala (areas: amygdaloid complex); STR, striatum (areas: striatum); THAL, thalamus (areas: dorsal thalamus, mediodorsal nucleus of thalamus); CBL/URL, cerebellum, upper rhombic lip (areas: cerebellum, cerebellar cortex, upper [rostral] rhombic lip). **B.** UMAP of single-nucleus RNA-sequencing (snRNA-seq) data from human postnatal donors (3 months - 13 years) colored by cell type. UMAP of snRNA-seq data with each nuclei's *ARHGEF6* expression. Expression values were clipped at the 99th percentile to improve color scale contrast and reduce the influence of outlier cells. 114,216 cells included from 18 samples across 9 unique subjects. EN-IT-Immature, intratelencephalic excitatory immature neurons; EN-L2_3-IT, layer 2/3 intratelencephalic excitatory neurons; EN-L4-IT, layer 4 intratelencephalic excitatory neurons; EN-L5-ET, layer 5 extratelencephalic excitatory neurons; EN-L5-IT, layer 5 intratelencephalic excitatory neurons; EN-L5_6-NP, layer 5/6 near-projecting excitatory neurons; EN-L6-CT, layer 6 corticothalamic excitatory neurons; EN-L6-IT, layer 6 intratelencephalic excitatory neurons; EN-L6b, layer 6b excitatory neurons; EN-Newborn, Newborn excitatory neurons; EN-Non-IT-Immature, immature non-intratelencephalic excitatory neuron;. IN-CGE-Immature, immature caudal ganglionic eminence-derived inhibitory neurons; IN-CGE-SNCG, immature caudal ganglionic eminence-derived gamma-synuclein inhibitory neurons; IN-CGE-VIP, caudal ganglionic eminence-derived vasoactive intestinal polypeptide inhibitory neurons; IN-MGE-Immature, immature medial ganglionic eminence-derived inhibitory neurons; IN-MGE-PV, medial ganglionic eminence-derived parvalbumin inhibitory neurons; IN-MGE-SST, medial ganglionic eminence-derived somatostatin inhibitory neurons; IN-Mix-LAMP5, mixed lysosomal-associated membrane protein family member 5 inhibitory neurons; IN-NCx_dGE-Immature, immature neocortex and dorsal ganglionic eminence-derived inhibitory neurons; IPC-EN, intermediate progenitor cell for excitatory neurons; OPC, oligodendrocyte precursor cells; RG-oRG, outer radial glial cells; RG-tRG, truncated radial glial cells; RG-vRG, ventricular radial glial cells; Tri-IPC, tripotential intermediate progenitor cells. **C**. UMAP of single-cell RNA-sequencing (scRNA-seq) data from ~8 week old (~P56) mice colored by cell type. UMAP of scRNA-seq data with *Arhgef6* expression for each cell cluster. 73347 cells included. PV, parvalbumin; SST, somatostatin; SST CHOLD, somatostatin and chondrolectin; LAMP5, lysosomal-associated membrane protein family member 5; SNCG, gamma-synuclein; VIP, vasoactive intestinal polypeptide; MEIS2, meis homeobox 2; CR, cajal-retzius cell; L2 IT ENTl, layer 2 intratelencephalic lateral entorhinal area; L2 IT ENTm, layer 2 intratelencephalic medial entorhinal area; L2/3 IT CTX, layer 2/3 intratelencephalic isocortex; L2/3 IT ENTl, layer 2/3 intratelencephalic lateral entorhinal area; L2/3 IT PPP, layer 2/3 intratelencephalic postsubiculum-presubiculum-parasubiculum; L2/3 IT RHP, layer 2/3 intratelencephalic retrohippocampal region; L3 IT ENT, layer 3 intratelencephalic entorhinal area; L4 RSP-ACA, layer 4 retrosplenial area-anterior cingulate area; L4/5 IT CTX, layer 4/5 intratelencephalic isocortex; L5 IT CTX, layer 5 intratelencephalic isocortex; L5 PPP, layer 5 postsubiculum-presubiculum-parasubiculum; L5 PT CTX, layer 5 pyramidal tract isocortex; L5/6 IT TPE-ENT, layer 5/6 intratelencephalic temporal association areas-perirhinal area-ectorhinal area-entorhinal area; L5/6 NP CTX, layer 5/6 near-projecting isocortex; L6 CT CTX, layer 6 corticothalamic isocortex; L6 IT CTX, layer 6 intratelencephalic isocortex; L6 IT ENTl, layer 6 intratelencephalic lateral entorhinal area; L6b CTX, layer 6b isocortex; L6b/CT ENT, layer 6b corticothalamic entorhinal area; NP PPP, near-projecting postsubiculum-presubiculum-parasubiculum; NP SUB, near-projecting subiculum; CT SUB, corticothalamic subiculum; Car3, carbonic anhydrase 3; SUB-Pros, subiculum-prosubiculum; CA1-ProS, field cornu ammonis 1-prosubiculum; CA2-IG-FC, field cornu ammonis 2-fasciola cinerea-indusium griseum; CA3, field cornu ammonis 3; DG, dentate gyrus; Astro, astrocyte; Oligo, oligodendrocyte; Micro-PVM, microglia/perivascular macrophage; Endo, endothelial cell; SMC-Peri, smooth muscle cell perivascular area; VLMC, vascular leptomeningeal cell. **D**. Representative *in situ* hybridization (ISH) images using an *Arhgef6* antisense RNA probe on coronal sections of embryonic (E) 14.5 wild-type (WT) mouse brains. LV, lateral ventricle; LGE, lateral ganglionic eminence; MGE, medial ganglionic eminence; CGE, caudal ganglionic eminence. Scale bar: 400 μm. **E**. Representative maximum intensity projection of z-stack images (30 serial image planes, z-step size = 1 μm) of the somatosensory cortex of postnatal (P) 45 *GAD67-eGFP* (left) and *GAD67-eGFP;Arhgef6-KO* mice (right). Scale bars, 200 μm. **F**. Average density of $eGFP^+$ GABAergic INs in the adult cortex in each of the 10 bins (shown in E). At least 3 distinct sections distributed along the anteroposterior axis from 3 different mice per genotype were analyzed. p-values (from bin 1 to 10) = (1) 0.004; (2) 0.058; (3) 0.032; (4) 0.012; (5) 0.033; (6) 0.004; (7) 0.005; (8) 0.005; (9) 0.043; (10) 0.044; (TOT) 0.005. **G**. Average percentage of $eGFP^+$ GABAergic INs in the adult cortex over the total number of cells. At least 3 distinct sections distributed along the anteroposterior axis from 3 different

mice per genotype were analyzed. p-values = 0.008. **H**. Representative maximum intensity projection of z-stack images (30 serial image planes, z-step size = 1 μm) of the hippocampus of P45 *GAD67-eGFP* (left) and *GAD67-eGFP;Arhgef6-KO* (right) mice. Scale bar, 100 μm. **I**. Average density of $eGFP^+$ GABAergic INs in the cornu ammonis region 1, 2, and 3 (CA1, CA2, CA3), and dentate gyrus (DG) regions and whole hippocampus. At least 3 distinct sections distributed along the anteroposterior axis from 3 different mice per genotype were analyzed. p-values = 0.097 (CA1); 0.00004 (CA2); 0.005 (CA3); 0.12 (DG); 0.044 (TOT). p-values were calculated using unpaired multiple t-tests corrected for False Discovery Rate (<1%) (F) and Holm-Šídák method (H). * = p< 0.05, ** = p< 0.01, *** = p< 0.001. Data are presented as mean ± SEM. Each dot represents one animal.

To further examine the cellular distribution of *ARHGEF6* expression, we next analyzed postnatal human cortical single-nucleus RNA sequencing (snRNA-seq) datasets spanning 3 months to 13 years of age (Wang et al., 2025)(Fig. 1B; Tab. S1). UMAP visualization of annotated cell populations showed that *ARHGEF6* is expressed within both neuronal and non-neuronal clusters (Fig. 1B). Within neuronal populations, *ARHGEF6* is enriched in specific GABAergic lineages, including MGE-derived parvalbumin (PV) INs and CGE-derived LAMP5-expressing INs (as shown in the magnified view in Fig. 1B). In contrast, excitatory cells exhibited comparatively lower *ARHGEF6* expression (Fig. 1B; Tab. S1). The detection of *ARHGEF6* expression in oligodendrocyte progenitor cells (OPCs) is consistent with the developmental origin of early OPC populations from ventral telencephalic progenitor domains, including the GEs (Cai et al., 2024). In addition to neural lineages, *ARHGEF6* is also expressed in immune-related cell types, including monocytes and monocyte progenitors, as similarly reported in broader transcriptomic datasets containing hematopoietic cells (The Human Protein Atlas; Uhlén et al., 2015; Uhlen et al., 2017). As microglia originate from yolk-sac-derived erythro-myeloid progenitors and share transcriptional programs with monocyte/macrophage lineages, the expression of *ARHGEF6* in this cell type is therefore consistent with its broader expression in cells of the myeloid/monocytic lineage.

Consistent with the early expression of *ARHGEF6* observed in the human developing telencephalon (Fig. 1A), when we examined *Arhgef6* expression in coronal sections of mouse embryonic brains using *in situ* hybridization (ISH) with a previously validated probe (Lein et al., 2007), the earliest detectable expression was observed around embryonic day (E) 14.5, with higher amounts in MGE and CGE and comparatively lower expression in the lateral ganglionic eminence (LGE) (Fig. 1C). The enrichment of *ARHGEF6* expression in inhibitory lineages was further supported by analysis of the publicly available Allen Brain Atlas single-cell RNA sequencing (scRNA-seq) dataset from adult (~P56) mouse cortex and hippocampus (Yao et al., 2021). Interestingly, as in the postnatal human brain, enrichment was detected in multiple subtypes of GABAergic INs, particularly MGE-derived PV+ cells and CGE-derived LAMP5+ INs (Fig. 1D; Tab. S2). Among excitatory populations, only CA3 pyramidal neurons and mossy cells exhibited expression levels comparable to those observed in inhibitory clusters (Fig. 1D, Tab. S2). Elevated expression within the CA3 stratum pyramidale was further confirmed by *in situ* hybridization (ISH) data available through the Allen Brain Atlas portal (Lein et al., 2007; Allen Institute for Brain Science, experiment RP_060315_04_C08). Consistent with these findings, previous studies have reported elevated *Arhgef6* expression in neuropil regions of the adult mouse hippocampus (Ramakers et al., 2012; Meyer, 2014).

Collectively, these findings suggest a previously undefined developmental role for this gene in the GABAergic telencephalic lineage that can be observed across species.

2. Arhgef6 deficiency reduces INs numbers in the adult cortex and hippocampus

Given that *ARHGEF6* expression is enriched in GABAergic INs in both the early embryonic and adult brains, we first aimed to determine whether adult mice exhibited any defects. To investigate the effect of *Arhgef6* deficiency on the inhibitory neuronal lineage, *Arhgef6-KO* mice (Ramakers et al., 2012) were crossed with the *GAD67-eGFP* reporter line (Tamamaki et al., 2003).

We then examined coronal sections of the sensory cortex and hippocampus from adult (P45) *GAD67-eGFP;Arhgef6-KO* mice and compared them with sections from *GAD67-eGFP* control mice. The brains of *GAD67-eGFP;Arhgef6-KO* mice exhibited a significant reduction in the number of $GAD67^+$ cells throughout the cortex (Fig. 1E-G), particularly in layers I, V-VI (corresponding to BIN 1, 6-8), and in the hippocampus, specifically within the CA2 and CA3 regions (Fig. 1H, I). The decrease in IN number within the CA2–CA3 regions occurs in an area enriched for *Arhgef6* expression (Lein et al., 2007; Allen Institute for Brain Science, experiment RP_060315_04_C08).

These findings suggest that the inhibitory balance may be altered in the adult mouse cortex and hippocampus, complementing previous findings and potentially explaining the cognitive impairment observed in mice (Ramakers et al., 2012).

3. Loss of Arhgef6 impairs cell survival during embryonic development

Our observation of a significant reduction in IN numbers in the adult cortex and hippocampus of *Arhgef6-KO* mice suggested that early developmental defects might underlie the adult phenotype. We hypothesized that the reduced number of adult cortical and hippocampal INs may, at least in part, result from impaired cell survival during development. To test this, we performed TUNEL staining on early (E14.5) (Fig. 2A) and late (E18.5) (Fig. 2D) embryonic brain sections from *Arhgef6-KO* and control mice.

At E14.5, TUNEL staining was analyzed in the neocortex and GE (Fig. 2A–C). No significant differences were detected in the cortex (Fig. 2B). In contrast, a significant increase in TUNEL punctae was observed in the GE of *Arhgef6-KO* embryos compared with controls (Fig. 2C), indicating elevated cell death in this region. We next examined apoptosis at a later embryonic (E18.5) timepoint, when the hippocampus is morphologically recognizable and the GE have largely regressed, and found a significant increase in TUNEL punctae in the hippocampus of *Arhgef6-KO* embryos (Fig. 2D, E).

These results suggest that loss of Arhgef6 impairs cell survival during embryonic development and may thereby contribute to the postnatal reduction in IN number.

4. Arhgef6 loss impairs tangential migration and directionality of GABAergic INs

Given the role of ARHGEF6 as a RAC1 GEF and the requirement of RAC1 signaling for IN migration (Vidaki et al., 2012; Chen et al., 2007; Tivodar et al., 2015), we investigated IN migration in *GAD67-eGFP;Arhgef6-KO* mice.

We examined coronal brain sections from E14.5 *GAD67-eGFP;Arhgef6-KO* embryos and quantified the density of INs undergoing tangential ventral-to-dorsal migration into the neocortex (Fig. 2F, G). The neocortex was subdivided into four equal regions, and IN numbers were quantified as previously described (Sun et al., 2021; Eid et al., 2025). We observed a significant reduction in the percentage of INs entering the neocortex in *GAD67-eGFP;Arhgef6-KO* embryos across all four defined regions (1–4) (Fig. 2G). We next analyzed the directionality of migrating INs by quantifying the orientation of their leading process relative to the tangential axis (Fig. 2H, I). In E14.5 *GAD67-eGFP;Arhgef6-KO* embryos, the proportion of cells oriented dorsally along the main tangential migratory stream (direction 1) was significantly reduced compared with controls (Fig. 2I). In contrast, a significant increase was observed in the percentage of INs oriented toward non-tangential directions (directions 2–4), including pial (2), ventral (3), and ventricular (4) orientations (Fig. 2I). In the same sections, we measured the length of the leading process in tangentially migrating INs and found a significant increase in *GAD67-eGFP;Arhgef6-KO* embryos compared with controls (Fig. 2J).

These findings support an IN migration defect in KO animals, likely reflecting impaired exit from the GE, as previously observed following RAC1 ablation (Chen et al., 2007; Vidaki et al., 2012), and indicate that *Arhgef6* deficiency disrupts leading-process directional coherence while

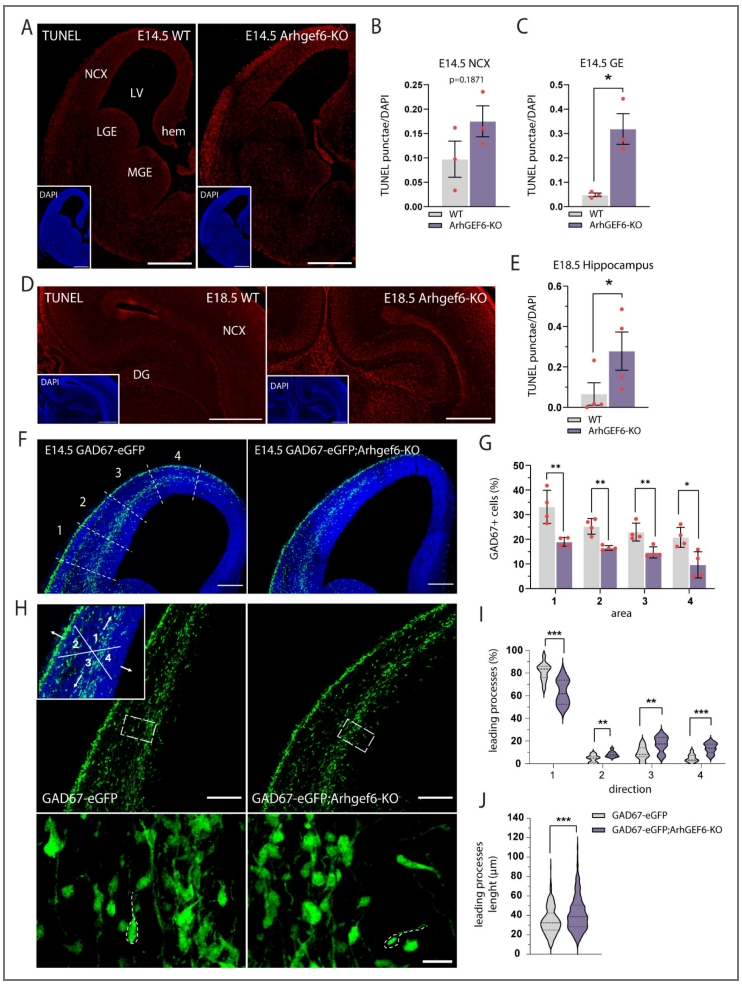

Figure 2. Murine embryonic INs show altered migratory patterns and reduced survival.

A. Representative maximum intensity projection of z-stack images (30 serial image planes, z-step size = 1 µm) of telencephalic coronal sections from E14.5 WT (left) and *Arhgef6-KO* (right) mouse stained for apoptotic nuclei using the TUNEL assay; insets show the corresponding DAPI staining highlighting overall cytoarchitecture. NCX, neocortex; LV, lateral ventricle; hem, cortical hem; LGE, lateral ganglionic eminence; MGE, medial ganglionic eminence. Scale bars, 500 µm. **B**, **C**. Average percentage of TUNEL punctae over the total number of nuclei. At least 3 distinct sections distributed along the anteroposterior axis from 3 different mice per genotype were analyzed. p-values = 0.1871 (E14.5 NCX); 0.0129 (E14.5 GE). **D**. Representative maximum intensity projection of z-stack images (30 serial image planes, z-step size = 1 µm) of hippocampal coronal sections from E18.5 WT (left) and *Arhgef6-KO* (right) mouse stained for apoptotic nuclei using the TUNEL assay; insets show the corresponding DAPI staining highlighting overall cytoarchitecture. NCX, neocortex; DG, dentate gyrus. Scale bars, 500 µm. **E**. Average percentage of TUNEL punctae over the total number of nuclei. At least 3 distinct sections distributed along the anteroposterior axis from 4 different mice per genotype were analyzed. p-value = 0.029 (E18.5 HIPP). **F**. Representative maximum intensity projection of z-stack images of neocortical coronal sections from E14.5 *GAD67-eGFP* (left) and *GAD67-eGFP;Arhgef6-KO* (right) stained for DAPI. The *GAD67-eGFP* shows the division of the neocortex into four areas of equal size (1, 2, 3, 4) used for the analysis (G). Scale bars, 200 µm. **G**. Average percentage of eGFP$^+$ GABAergic INs over the total number of cells in each of the four areas. At least 3 distinct sections distributed along the anteroposterior axis from 4 different mice per genotype were analyzed. p-value (from area 1 to 4) = 0.008 (1); 0.006 (2); 0.008 (3); 0.0119 (4). **H**. Representative maximum intensity projection of z-stack images of neocortices from E14.5 *GAD67-eGFP* (left) and *GAD67-eGFP;Arhgef6-KO* (right) embryos; the inset in the *GAD67-eGFP* shows a schematic representation of the four directions analysed: tangential-dorsal (1), pial (2), ventral (3), ventricular (4). Scale bars, 150 µm. Below, higher magnification of the regions outlined by dashed white boxes, showing different orientations of the leading processes of INs. Scale bar, 50 µm. **I**. Percentage of eGFP$^+$ GABAergic INs with the leading processes oriented in each of the 4 directions. p-values (from direction 1 to 4) = 0.0001 (1); 0.002 (2); 0.003 (3); 0.00004 (4). **J**. Average length (µm) of leading processes of migrating eGFP$^+$ GABAergic INs. p-value < 0.001. p-values were calculated using unpaired t-test (B, C, E, J), unpaired multiple t-tests corrected for False Discovery Rate (<1%) (G, I). * = p< 0.05, ** = p< 0.01, *** = p< 0.001. Data are presented as mean ± SEM. Each dot represents one animal. Violin plots show the distribution of values with median and quartiles indicated.

inducing morphological alterations in tangentially migrating cortical INs.

5. Arhgef6 deficiency impairs neurite branching in hippocampal INs

Given the well-established role of RAC1 in neurite outgrowth (Liaci et al., 2021), we asked whether reduced RAC1 pathway activity resulting from Arhgef6 loss (Ramakers et al., 2012) affects the morphology of GABAergic INs. To test this, we prepared primary dissociated hippocampal cultures from P0 *GAD67-eGFP* and *GAD67-eGFP;Arhgef6-KO* pups and maintained them for 10 days *in vitro* (DIV) (Fig. 3A).

At 10 DIV, we assessed neurite length, arborization, and overall complexity using Sholl analysis. Compared with controls, *Arhgef6-KO* GAD67$^+$ neurons showed fewer intersections between 80 and 200 µm from the soma, whereas control neurons displayed a progressive increase in intersections with distance, up to 200 µm (Fig. 3B). No significant differences were detected in the soma diameter, number of primary neurites, and length of the longest neurite between genotypes (Fig. S1A-C).

These results suggest that *Arhgef6* loss compromises distal branching and neurite complexity.

6. Arhgef6 loss reduces INs excitability

Previous studies have shown that loss of Arhgef6 in hippocampal pyramidal neurons alters long-term potentiation (LTP) and long-term depression (LTD) in the Schaffer collateral–CA1 pathway (Ramakers et al., 2012). To assess whether Arhgef6 depletion also affects IN electrophysiological properties, we performed whole-cell patch-clamp recordings from GAD67$^+$ cells in acute slices from adult *GAD67-eGFP* and *GAD67-eGFP;Arhgef6-KO* mice.

Representative traces of evoked action potentials revealed differences in baseline firing and firing frequency between genotypes (Fig. 3C). *Arhgef6-KO* INs displayed a reduced firing rate in response to incremental current injections (0–300 pA), with significant differences emerging from 70 pA onward (Fig. 3D). We quantified instantaneous firing frequency at spike train onset (f_o) and steady state (f_{ss}) to evaluate spike frequency adaptation. Both f_o and f_{ss} were significantly reduced at 120 and 280 pA, while only f_{ss} was reduced at 180 pA (Fig. 3E, F).

In contrast, input resistance (R_{in}), resting membrane voltage (V_{rest}), membrane capacitance, and rheobase were unchanged (Fig. S1D, F, G, H). Similarly, single action potential properties, including peak amplitude, half-width, maximal rising slope, and maximal repolarizing slope, did not differ between genotypes (Fig. S1I, J, K, L).

Overall, these data indicate that Arhgef6 loss reduces IN firing output, consistent with a hypoexcitable phenotype, without overt changes in passive membrane properties or single action potential waveform.

7. Establishment of an *ARHGEF6-KO* human iPSC line and cytoskeletal phenotyping in NPCs

To investigate the role of *ARHGEF6* in human development we generated an *ARHGEF6-KO* human induced pluripotent stem cell (hiPSC) line using CRISPR–Cas9.

A commercially available male hiPSC line (ATCC-DYS0100) was targeted with a crRNA designed to disrupt exon 3, the first exon common to all *ARHGEF6* isoforms, resulting in a one–base pair deletion that introduced a frameshift mutation (Fig. S2A). As a control, we generated an RNP negative line from the same parental line using a non-targeting crRNA. The *ARHGEF6-KO* line maintained pluripotent stem cell state, as indicated by co-expression of OCT4 and SOX2 (Fig. S2B). Sequencing confirmed the absence of mutations at the three top predicted off-target exonic sites in the mutant line (Fig. S2C). *ARHGEF6-KO* hiPSC robustly differentiated into embryoid bodies containing derivatives of all three germ layers (ACTA2$^+$ mesodermal derivatives,

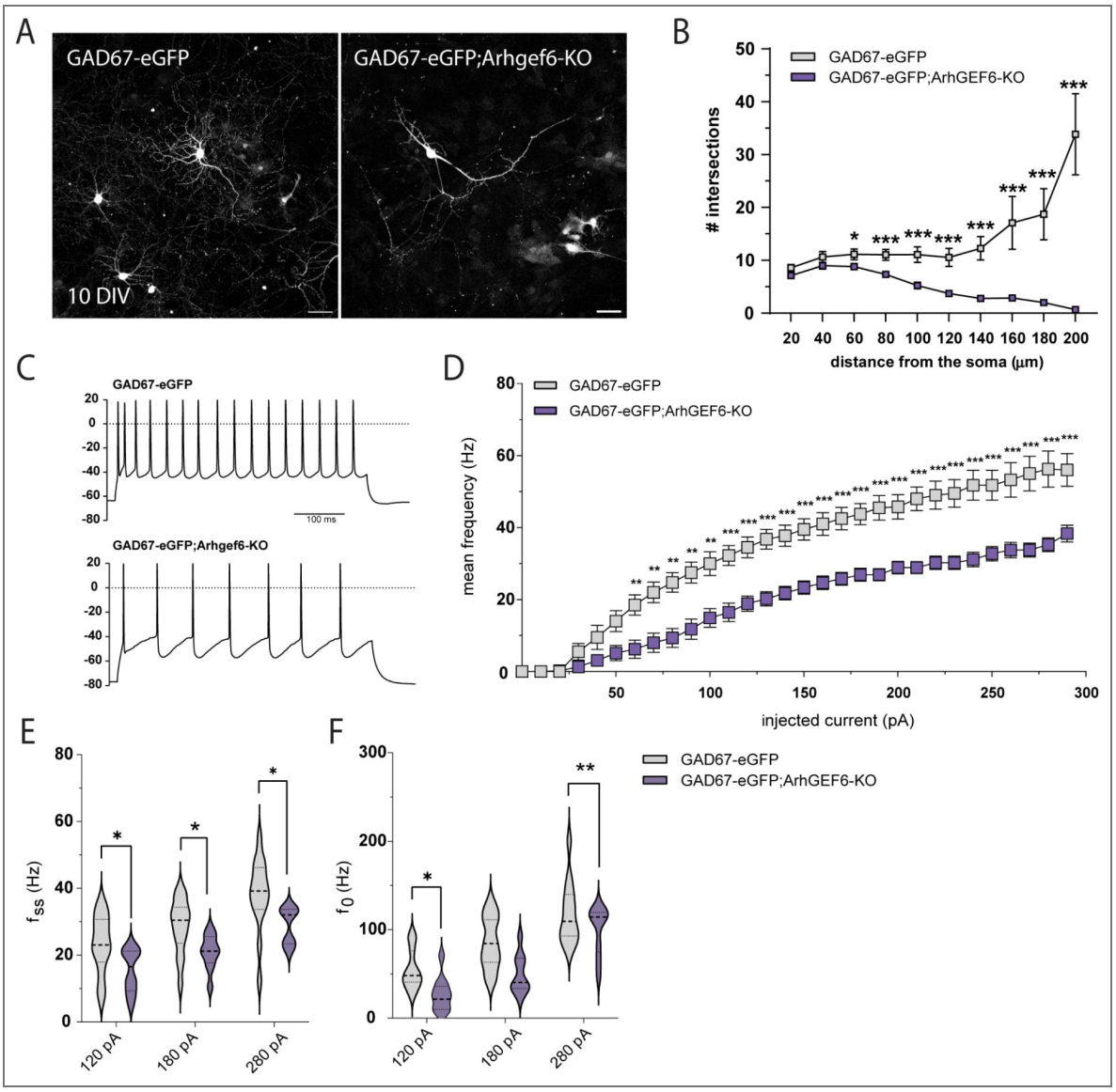

Figure 3. ***Arhgef6-KO*** **INs exhibit simpler branching and reduced excitability.**

A. Representative micrographs of eGFP$^+$ primary murine hippocampal INs from *GAD67-eGFP* (left) and *GAD67-eGFP;Arhgef6-KO* (right) after 10 days *in vitro* (DIV). Scale bars, 20 µm. **B**. Sholl analysis showing the overall complexity of arborization in *GAD67-eGFP* and *GAD67-eGFP;Arhgef6-KO* primary INs after 10 DIV. p-values (from 20 to 200 µm) = 0.023 (20 µm), 0.054 (40 µm), 0.019 (60 µm), 0.0009 (80 µm), 0.0003 (100 µm), 0.0003 (120 µm), 0.0003 (140 µm), 0.0009 (160 µm), 0.0007 (180 µm), 0.0003 (200 µm). Around 30 neurons from 2 independent primary cultures were analyzed for each genotype. **C**. Representative whole-cell current clamp recordings of action potentials evoked by 100 pA step current for *GAD67-eGFP* (top) and *GAD67-eGFP;Arhgef6-KO* (bottom) INs. **D**. Average firing frequency vs. current relationships recorded in *GAD67-eGFP* and *GAD67-eGFP;Arhgef6-KO* INs in response to a set of injected current steps (from 0 to 300 pA; 10 pA steps). p-values (from 0 to 300 pA) = 0.999 (0 pA), >0.999 (10 pA), 0.999 (20 pA), 0.708 (30 pA), 0.368 (40 pA), 0.102 (50 pA), 0.008 (60 pA), 0.002 (70 pA), 0.0004 (80 pA), 0.0004 (90 pA), 0.0006 (100 pA), 0.0004 (110 pA), 0.0004 (120 pA), 0.0002 (130 pA), 0.0003 (140 pA), 0.0003 (150 pA), 0.0003 (160 pA), 0.0002 (170 pA), 0.0002 (180 pA), 0.00002 (190 pA), 0.0002 (200 pA), 0.00001 (210 pA), 0.00002 (220 pA), 0.00001 (230 pA), 0.000002 (240 pA), 0.00002 (250 pA), 0.00001 (260 pA), 0.000002 (270 pA), 0.000002 (280 pA), 0.0004 (290 pA). Patch-clamp recordings were obtained from 11 cells from 4 *GAD67-eGFP* mice and 12 cells from 4 *GAD67-eGFP;Arhgef6-KO* mice. **E**. Mean firing frequency at steady state (f_{ss}) in response to current injections (120, 180, and 280 pA) in *GAD67-eGFP* and *GAD67-eGFP;Arhgef6-KO* INs. p-values: 0.039 (120 pA), 0.039 (180 pA), 0.024 (280 pA). **F**. Mean initial firing frequency (f_0) measured at the onset of current injection in *GAD67-eGFP* and *GAD67-eGFP;Arhgef6-KO* INs at 120, 180, and 280 pA. p-values: 0.034 (120 pA), 0.0098 (180 pA), 0.127 (280 pA). p-values were calculated using unpaired multiple t-tests corrected for False Discovery Rate (<1%) (B), and Holm-Šídák method (D, E, F). * = p< 0.05, ** = p< 0.01, *** = p< 0.001. Data are presented as mean ± SEM. Violin plots show the distribution of values with median and quartiles indicated.

GATA4⁺ endoderm, and MAP2⁺ neuroectoderm), indicating preserved developmental potential (Fig. S2D), as well as neural progenitor cells (NPCs) coexpressing NESTIN, SOX2 and the radial glia markers PAX6 and FABP7 (Fig. S2E).

To assess the impact of RAC1 pathway disruption on cytoskeletal dynamics, we performed Phalloidin-FITC staining on NPCs to visualize F-actin filaments and evaluate cytoskeletal organization (Fig. S2F). We quantified the anisotropy index, which reflects the degree of alignment of F-actin fibers: cells with a greater proportion of fibers oriented along a common axis exhibit higher anisotropy. *ARHGEF6-KO* cells showed a significantly increased anisotropy index (Fig. S2G), indicating a more "aligned" actin cytoskeleton than controls. In parallel, we quantified Phalloidin fluorescence to assess total polymerized actin and found that *ARHGEF6-KO* cells displayed a significant reduction in F-actin content compared with controls (Fig. S2H).

8. ARHGEF6 deficiency impairs ventral forebrain organoid growth and shape

To investigate ARHGEF6 function during human subpallial (ventral telencephalic) development, we used the *ARHGEF6-KO* and RNP negative control hiPSC lines to generate patterned ventral forebrain organoids using a drug-treatment regimen that augments SHH signaling while concurrently inhibiting WNT signaling, as previously described (Bagley et al., 2017; Birey et al., 2017, 2022).

At the end of the patterning phase (day 24), brightfield microscopy revealed multiple germinal zone-like (rosettes) in organoids from both genotypes. At the two-month time point, ventral *ARHGEF6-KO* organoids were markedly smaller than isogenic controls, showing a significant reduction in area and density (Fig. 4A–C). In addition, *ARHGEF6-KO* organoids displayed a clear change in gross morphology, with an increased aspect ratio (a more elongated shape) and reduced roundness (less circular/compact profiles) compared with controls (Fig. 4A, D, E).

9. ARHGEF6 loss alters ventral forebrain organoid development

NKX2.1 expression is a hallmark of ventral telencephalic/MGE identity and is widely used to assess successful generation of MGE-like tissue, a principal source of cortical INs in humans (Hansen et al., 2013; Ma et al., 2013). Immunostaining for NKX2.1 in organoids from both genotypes confirmed successful ventral patterning (Fig. 4F).

To investigate cellular mechanisms that could contribute to the reduced size of *ARHGEF6-KO* organoids, we next assessed survival and cellular composition at one month. TUNEL staining revealed a significant increase in apoptotic cells in *ARHGEF6-KO* organoids (Fig. 4G, H). TUNEL punctae were distributed throughout the tissue and were particularly enriched in inter-rosette regions, suggesting that cell death may preferentially affect post-mitotic populations rather than proliferative progenitors within germinal zones. Consistent with this, quantification showed reduced numbers of both SOX2⁺ progenitors and NEUN⁺ neurons in *ARHGEF6-KO* organoids, with a more pronounced decrease in NEUN⁺ cells (Fig. 4I-K).

Collectively, these data indicate that ARHGEF6 loss is associated with a reduced NKX2.1⁺ progenitor pool and increased cell death, which may contribute to reduced neuronal output and could reflect impaired neurogenesis and/or decreased neuronal survival in ventral forebrain organoids.

10. *ARHGEF6-KO* INs exhibit impaired migration in dorsal-ventral assembloids

To assess the impact of ARHGEF6 loss on IN migration in a human context, we used dorsal–ventral assembloids to model ventral-to-dorsal migration. We transduced ventral organoids with lenti-DLX1/2b:eGFP to label INs and, at two months, fused them with dorsal organoids to generate dorsal–ventral assembloids, following established protocols (Bagley et al., 2017; Birey et al., 2017, 2022) (Fig. 5A). This system recapitulates migration of multiple MGE-derived IN subtypes and their characteristic saltatory behavior, consisting of alternating phases of rapid

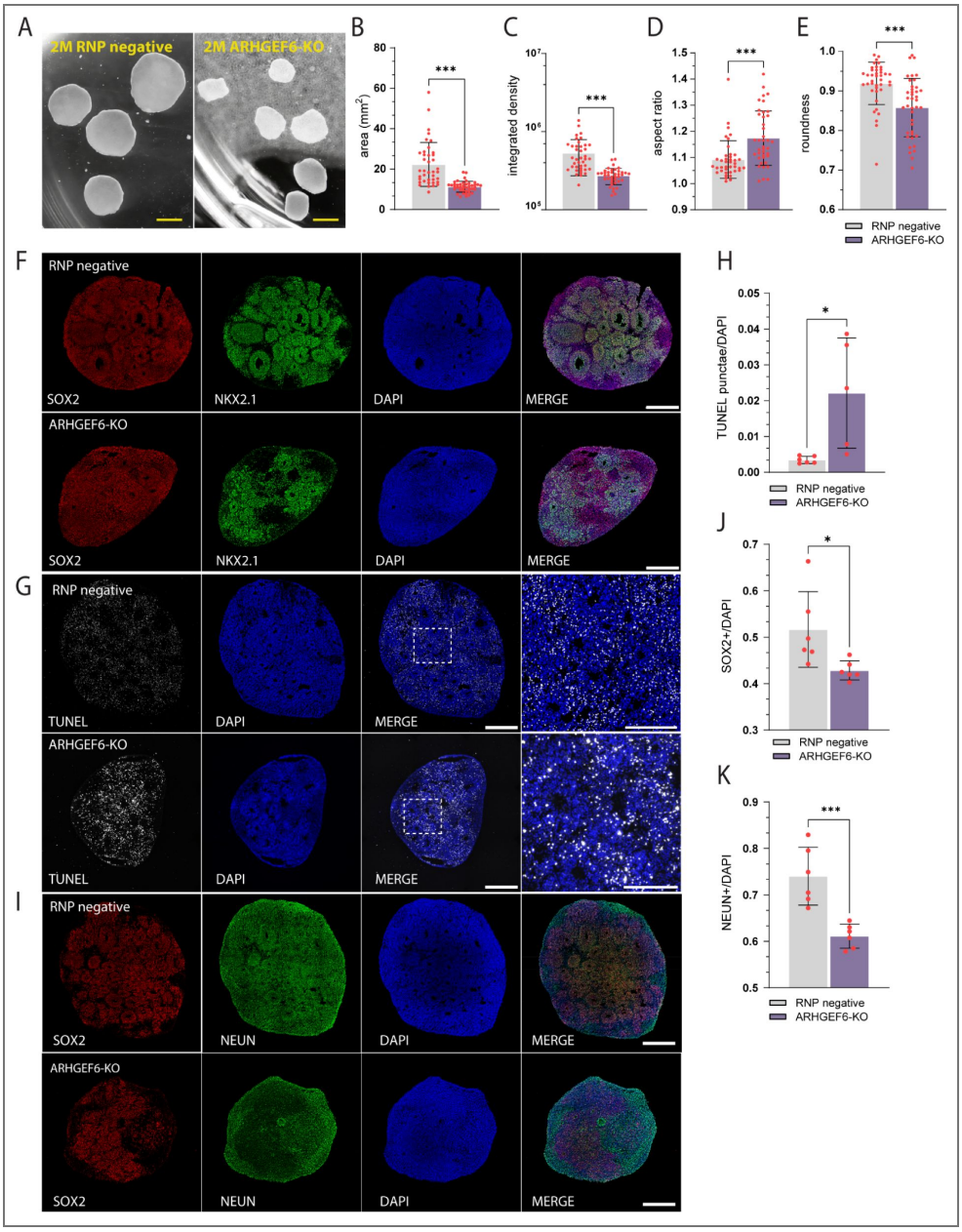

Figure 4. Characterization of ventral forebrain organoids from *ARHGEF6-KO* hiPSCs.

A. Representative brightfield images of RNP negative (control) and *ARHGEF6-KO* human induced pluripotent stem cell (hiPSC)–derived organoids at 2 months (2M) of differentiation. Scale bars, 4 mm. **B–E**. Quantification of organoid size, density, and shape descriptors. 3 different batches of differentiation were analyzed. p-values = <0.0001 (area), <0.0001 (integrated density), <0.0001 (aspect ratio), <0.0001 (roundness). **F**. Immunofluorescence staining of 1-month ventral forebrain organoids showing expression of the neural progenitor marker SOX2 and the ventral telencephalic marker NKX2.1, confirming ventral forebrain identity. Nuclei are labeled with DAPI. Scale bars, 500 µm. **G**. Detection of apoptotic nuclei by TUNEL assay in RNP negative and *ARHGEF6-KO* 1-month organoids. Right panels show higher magnification of the boxed regions. Nuclei are labeled with DAPI. Scale bars, 500 µm. **H**. Average percentage of TUNEL punctae over the total number of nuclei. p-value = 0.015. At least 5 distinct sections from 5 different organoids per genotype from 3 different batches of differentiation were analyzed. **I**. Immunofluorescence staining for the neural progenitor marker SOX2 and the neuronal marker NEUN, indicating neuronal differentiation in RNP negative and *ARHGEF6-KO* 1-month organoids. Nuclei are labeled with DAPI. Scale bars, 500 µm. **J, K**. Quantification of $SOX2^+$ progenitors and $NEUN^+$ neurons normalized to the total number of nuclei in RNP negative and *ARHGEF6-KO* organoids. p-values = 0.028 (J), 0.0008 (K). At least 5 distinct sections from 6 different organoids per genotype from 3 different batches of differentiation were analyzed. p-values were calculated using unpaired t-test. * = p< 0.05, ** = p< 0.01, *** = p< 0.001. Data are presented as mean ± SEM. Each dot represents one organoid.

movement and pauses (Birey et al., 2017). To examine the behavior of migrating INs, we performed time-lapse recordings of dorsal-ventral assembloids cultured for 1-2 weeks after fusion (Fig. 5B; Video S1, 2). The eGFP$^+$ ventral region was readily distinguishable from the dorsal region, allowing for clear visualization of the morphology of sparsely labeled migrating INs.

The fraction of DLX1/2b-eGFP$^+$ INs migrating along the ventral-to-dorsal axis was comparable between genotypes (Fig. 5C). However, trajectory analysis revealed that *ARHGEF6-KO* INs migrated less directly, as reflected by reduced path directness (linear distance/path length) (Fig. 5D). Consistent with this, time-lapse imaging showed a reduction in overall average migration velocity (Fig. 5E) and altered saltatory dynamics (Birey et al., 2017), including fewer saltations, prolonged saltation events, and shorter saltation length (Fig. 5F–H).

Collectively, these results indicate that ARHGEF6 loss impairs the efficiency and coordination of IN migration in dorsal–ventral assembloids, despite preserved overall orientation.

11. *ARHGEF6-KO* INs show reduced branching

Given the morphological abnormalities observed in Arhgef6-deficient INs *in vivo*, we asked whether ARHGEF6 loss similarly affects neurite arborization in human INs. We therefore quantified neurite branching of DLX1/2b-eGFP$^+$ INs from ventral organoids cultured for four months using Sholl analysis (Fig. 6A). Compared with RNP negative controls, *ARHGEF6-KO* INs exhibited a reduced number of intersections in the proximal compartment (approximately 0–50 µm from the soma), whereas branching at larger distances was largely comparable between genotypes (Fig. 6B).

The apparent discrepancy between the proximal branching defect observed in organoid-derived INs and the reduction of distal branching detected in primary neuronal cultures likely reflects differences in developmental maturation. Primary neurons have already undergone early stages of neurite specification *in vivo* prior to dissociation, revealing defects mainly in distal arborization. In contrast, organoid-derived neurons establish their neuritic arbor entirely *in vitro*, allowing earlier defects in proximal branching to become apparent. This result reinforces our previous findings, confirming that loss of ARHGEF6 reduces neurite complexity in both mouse and human models.

12. *ARHGEF6-KO* neurons exhibit altered growth cones morphology

Because migration and neurite branching depend on RAC1-driven cytoskeletal remodeling at the growth cone, we next asked whether ARHGEF6 loss impacts growth cone architecture in human neurons.

To visualize F-actin dynamics in live cells, we transduced one-month forebrain organoids with lenti–LifeAct-GFP and plated organoid-derived cells onto Geltrex-coated surfaces to promote adhesion and process extension. We then performed time-lapse imaging to monitor F-actin–rich growth cones in migrating neurons (Fig. 6C, D; Video S3, 4). Quantitative analysis showed that *ARHGEF6-KO* growth cones had reduced circularity and solidity (Fig. 6E, F), indicating a less compact morphology with a more elongated, protrusion-rich outline. In contrast, the average rate of size change over the imaging period was comparable between genotypes (Fig. 6G).

Collectively, these findings support a model in which ARHGEF6 contributes to cytoskeletal organization at the growth cone, providing a potential cellular basis for the migration and maturation deficits observed upon its loss.

Discussion

In this study, we identify ARHGEF6 as a conserved regulator of forebrain GABAergic IN development in both mouse and human iPSC-derived systems, and show that loss of ARHGEF6 consistently impairs processes central to inhibitory circuit assembly, including migration, neurite branching, growth cone organization, electrophysiological maturation, and survival. These findings are particularly relevant given the established importance of GABAergic INs in the assembly and function of forebrain circuits. Although they represent only a minority of the total

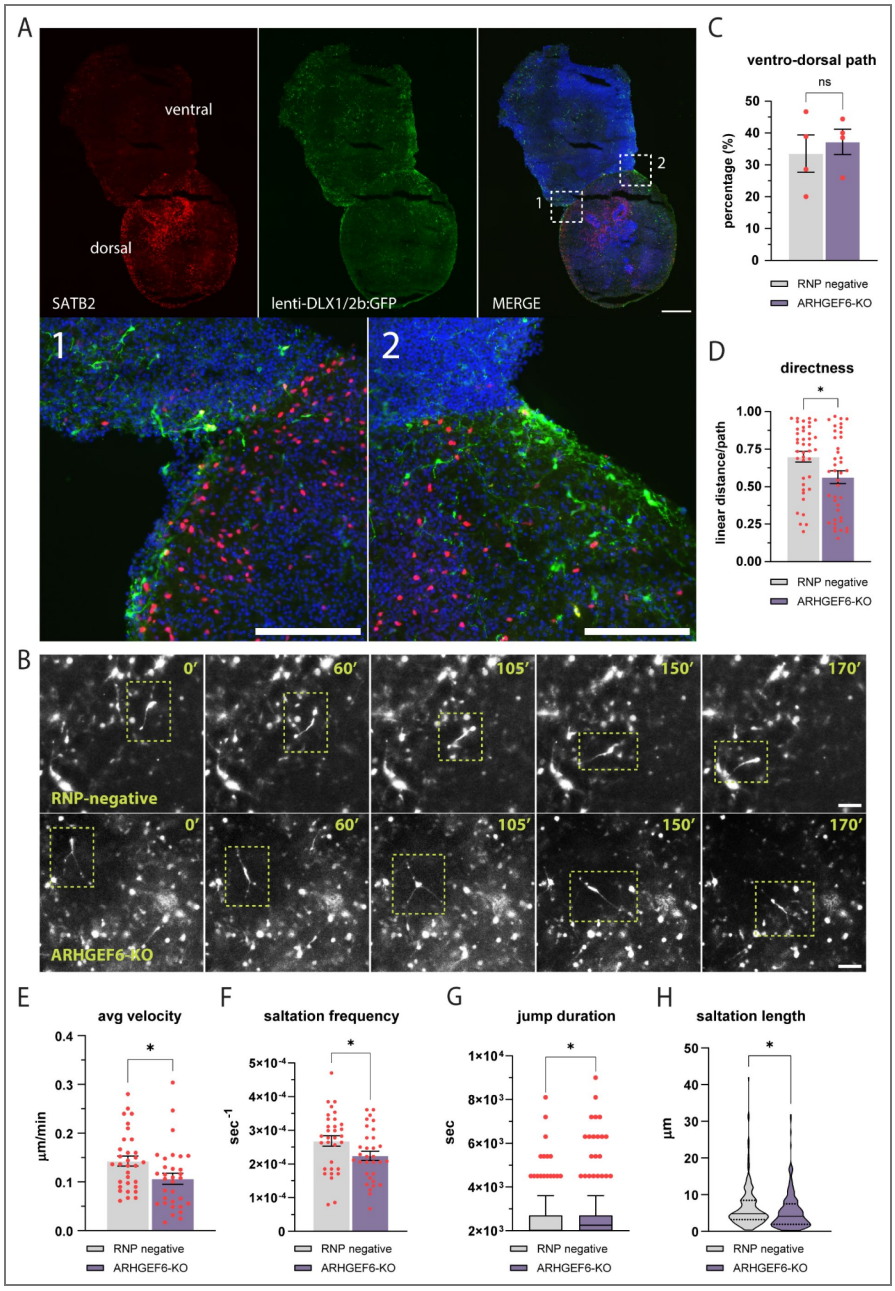

Figure 5. Impaired migration dynamics of DLX1/2b-GFP–labeled INs in ARHGEF6-deficient dorsal–ventral forebrain assembloids.

A. Characterization of a fused dorsal–ventral assembloids by immunofluorescence. The dorsal compartment is labeled by SATB2 (red), whereas the ventral compartment expresses lenti-DLX1/2b-eGFP (green), marking ventral telencephalic IN progenitors. Nuclei are counterstained with DAPI (blue). Insets (1–2) show higher magnification of regions at the dorsal–ventral interface where GFP$^+$ INs migrate from the ventral to the dorsal compartment. Scale bars, 500 µm, 150 (insets) µm. **B**. Representative frames from time-lapse imaging of migrating DLX1/2b-eGFP+ INs in fused assembloids, showing the saltatory migration behavior of individual INs in RNP negative (control) and *ARHGEF6-KO* assembloids. The tracked neuron is highlighted by dashed boxes in each frame. Scale bars, 100 µm. **C**. Quantification of the percentage of DLX1/2b-eGFP$^+$ INs in the ventral compartment migrating toward the dorsal compartment. p-value = 0.624. **D–H**. Quantitative analysis of migration parameters of individual DLX1/2b-eGFP$^+$ INs in RNP negative and *ARHGEF6-KO* assembloids. p-values = 0.016 (directness), 0.021 (average velocity), 0.038 (saltation frequency), 0.039 (jump (saltation event) duration), 0.043 (saltation length). At least 32 neurons from 3 independent assembloids per genotype from 2 different batches of differentiation were analyzed. p-values were calculated using unpaired t-test. * = p< 0.05, ** = p< 0.01, *** = p< 0.001. Data are presented as mean ± SEM. Each dot represents one tracked neuron. Violin plots show the distribution of values with median and quartiles indicated.

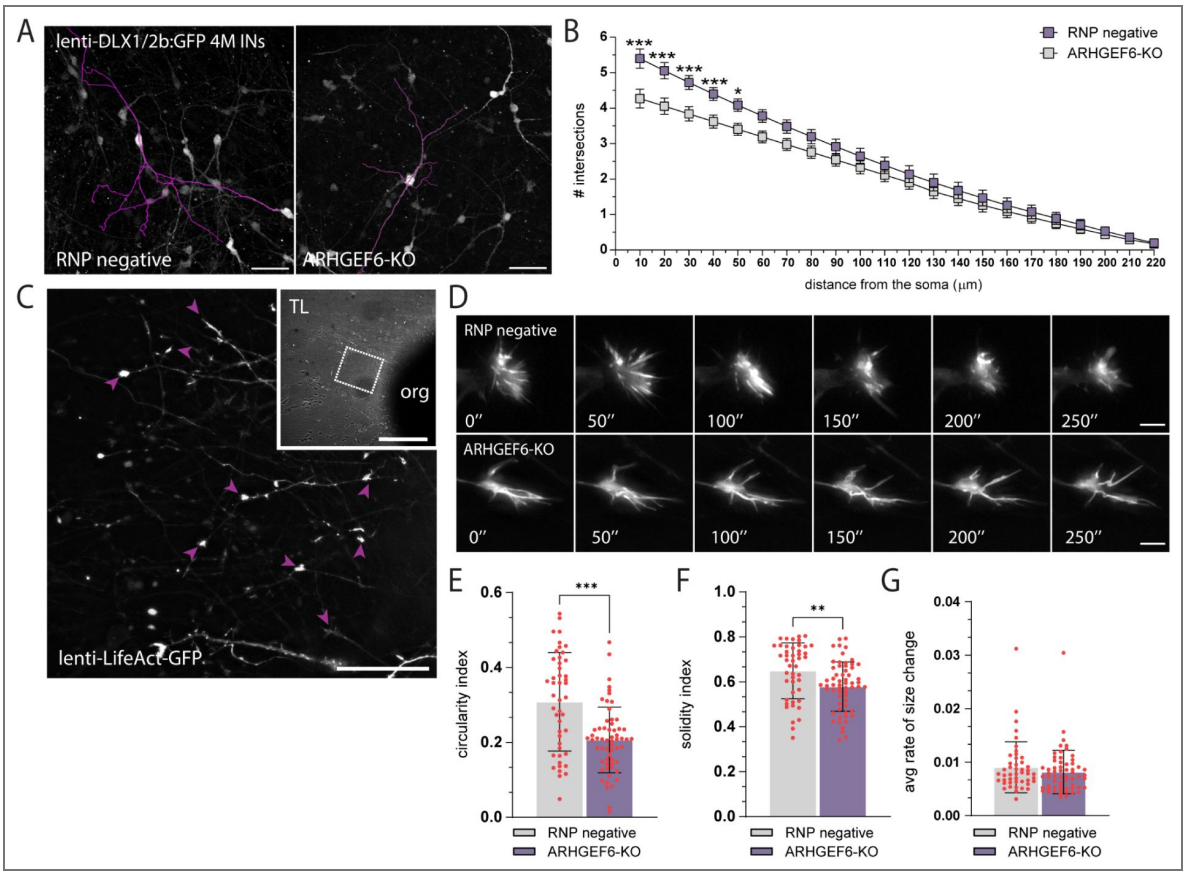

Figure 6. Impaired neuritogenesis and disrupted growth cone morphology in *ARHGEF6-KO* human neurons.

A. Representative fluorescence images of reconstructed individual DLX1/2b-eGFP$^+$ INs (purple skeletonization) from 4 months (4M) RNP negative (left) and *ARHGEF6-KO* (right) forebrain ventral organoids. Scale bar, 70 μm. **B**. Sholl analysis quantifying neurite length/complexity as the number of intersections across concentric radii (10–220 μm). p-values (from 10 to 220 μm) = 0.000003 (10 μm), 0.00003 (20 μm), 0.0003 (30 μm), 0.002 (40 μm), 0.008 (50 μm), 0.027 (60 μm), 0.070 (70 μm), 0.148 (80 μm), 0.263 (90 μm), 0.403 (100 μm), 0.548 (110 μm), 0.615 (120 μm), 0.569 (130 μm), 0.615 (140 μm), 0.679 (150 μm), 0.783 (160 μm), 0.814 (170 μm), 0.835 (180 μm), 0.848 (190 μm), 0.848 (200 μm), 0.848 (210 μm), 0.848 (220 μm). **C**. Representative image of neurites extending from a 1-month forebrain organoids transduced with LifeAct-GFP lentivirus. The inset contains a transmitted-light (TL) image of the organoid (org) plated showing migrating neurons and neuronal extensions. LifeAct-GFP$^+$ growth cones are indicated by purple arrowheads. Scale bars, 50 μm, 200 μm (inset). **D**. Representative frames from time-lapse recordings of growth cones from RNP negative (top) and *ARHGEF6-KO* (bottom) LifeAct-GFP$^+$ growth cones at 0′′, 50′′, 100′′, 150′′, 200′′, and 250′′. Scale bar, 5 μm. **E–G**. Quantification of growth cone shape descriptors and dynamics. p-values = < 0.001 (average circularity index), 0.003 (average solidity index), 0.299 (average rate of change in size). A total of 43 growth cones from 6 RNP negative organoids and 60 growth cones from 6 *ARHGEF6-KO* organoids, derived from 2 independent differentiation batches, were analyzed. Each dot represents one tracked growth cone. Data are shown as mean ± SEM. Statistical comparisons were performed using unpaired t-tests (E-G) and unpaired multiple t-tests corrected for False Discovery Rate (<1%) (B). *p < 0.05, **p < 0.01, ***p < 0.001.

neuronal population, cortical and hippocampal INs regulate virtually all aspects of local circuit maturation and activity through their morphological, neurochemical, and functional diversity (Pelkey et al., 2017; Lim et al., 2018; Kirmse et al., 2022). Developmental disruption of IN number, positioning, subtype composition, or intrinsic properties can therefore produce long-lasting circuit-level consequences and has been implicated in multiple neurodevelopmental disorders (Marín, 2012; Yang et al., 2022; Marilovtseva et al., 2025).

The molecular function of ARHGEF6 previously described in literature is highly consistent with the phenotypes observed here. Cell migration, neuritogenesis, and growth cone navigation all require tight control of the actin cytoskeleton, a process largely governed by Rho-family GTPases and their regulators. In line with this, ARHGEF6-deficient INs showed abnormalities in multiple cytoskeleton-dependent processes, including reduced migration directness and speed, reduced neurite complexity, and abnormal growth cone morphology. These phenotypes were observed not only in the mouse model but also in dorsal–ventral assembloids, indicating that the function of ARHGEF6 in IN development is conserved across species. The concordance between mouse and human systems is particularly important given the longstanding uncertainty surrounding the relevance of ARHGEF6 dysfunction to human disease.

Our human assembloid experiments extend the mouse findings by showing that *ARHGEF6-KO* INs exhibit reduced migration efficiency and impaired saltatory behavior (Birey et al., 2017). This parallels our *in vivo* observations in embryonic mouse brain, where fewer INs entered the cortex and their leading processes showed reduced coherence along the tangential axis. Likewise, branching defects were observed in both species, although they were more distal in mouse primary neurons and more proximal in organoid-derived human INs. We interpret this apparent discrepancy as a difference in developmental context rather than a contradiction, as both systems converge on the same conclusion: loss of ARHGEF6 reduces IN neuritic complexity.

A further key finding of our study is the increase in developmental cell death in the absence of ARHGEF6. In the mouse, apoptosis was elevated in the GEs at E14.5 and in the hippocampus at E18.5; in human ventral organoids, TUNEL-positive cells were also increased, particularly outside rosette-like proliferative zones. At present, we cannot determine whether this survival defect is entirely cell-autonomous or also influenced by altered network activity. However, neuronal survival during development is shaped not only by an intrinsic basal rate of cell death but also, to a large extent, by activity-dependent mechanisms (Heck et al., 2008; Southwell et al., 2012; Wong et al., 2018; Causeret et al., 2018; Bitzenhofer et al., 2021), and INs themselves contribute critically to early cortical activity patterns, including spontaneous bursts and oscillations (Bonifazi et al., 2009; Isaacson & Scanziani, 2011; Blanquie et al., 2017). Because we observe altered migration, reduced IN numbers, and decreased firing in *Arhgef6* mutants, it is plausible that mutant INs fail to appropriately engage in immature activity patterns and are thereby rendered more vulnerable to developmental apoptosis.

This interpretation is reinforced by our electrophysiological data. In postnatal *Arhgef6* mutant mice, hippocampal INs showed a reduction in firing rate in response to current injection, as well as altered spike-frequency adaptation, overall consistent with a hypoexcitable phenotype. These changes occurred in the absence of major differences in passive membrane properties or single action potential waveform, suggesting a selective alteration in intrinsic firing behavior rather than a general loss of membrane integrity. Such a change is likely to affect local inhibitory function and could sum up with the synaptic plasticity defects already described in *Arhgef6*-deficient pyramidal neurons, including reduced LTP and enhanced LTD at the Schaffer collateral–CA1 synapse (Ramakers et al., 2012). Together, these findings support the idea that ARHGEF6 deficiency disrupts both excitatory and inhibitory components of the hippocampal circuitry, thereby increasing the likelihood of an excitation/inhibition imbalance relevant to cognitive dysfunction.

Our human organoid models also suggest that ARHGEF6 may act at earlier developmental stages, before overt IN migration begins. *ARHGEF6*-mutant ventral forebrain organoids were smaller, more elongated, less compact, and showed increased apoptosis along with reduced numbers of $SOX2^+$ progenitors and $NEUN^+$ neurons, raising the possibility of impaired progenitor maintenance and delayed neurogenesis. This is consistent with emerging evidence that Rho

GTPases and their regulators contribute not only to migration and neurite dynamics, but also to neural progenitor proliferation, polarity, and fate decisions (Lian et al., 2019; Vidaki et al., 2012; Hass et al., 2025). More broadly, Rho GTPase signaling have been implicated in neurogenesis and microcephaly-associated phenotypes (Zuo et al., 2014; Jaffe and Hall, 2005; Reijnders et al., 2017; Chen et al., 2009; Duerinckx and Abramowicz, 2018). Although *ARHGEF6* mutations have not been clearly associated with microcephaly in patients, possibly due to the rarity of the condition, our organoid data suggest that ARHGEF6 may nonetheless influence early neurodevelopmental processes, including progenitor maintenance and neuronal output.

All these developmental findings are particularly relevant in light of the unresolved genetics of *ARHGEF6*-associated ID. *ARHGEF6* was initially proposed as the causal gene for nonsyndromic XLID46 (Kutsche et al., 2000; Yntema et al., 1998), but subsequent re-evaluation questioned this association because some reported variants are also present in apparently unaffected individuals and because direct functional evidence in human neurons has been limited (Piton et al., 2013). Clinical curation efforts have accordingly downgraded the evidence supporting a direct *ARHGEF6*–XLID46 relationship. However, the rarity of this condition makes it unlikely that human genetics alone will soon resolve the issue. In this context, our work provides precisely the kind of evidence that has been lacking: direct functional data in mouse and human inhibitory neurons showing that ARHGEF6 loss impairs core developmental processes highly relevant to cognition.

Finally, our results fit within a broader framework in which dysregulation of Rho GTPase signaling contributes to ID and related neurodevelopmental disorders. Variants in RAC1 itself cause a neurodevelopmental syndrome with ID, cortical malformations, and developmental delay, with both dominant-negative and gain-of-function alleles described (Banka et al., 2022; Haugh et al., 2021; Nishikawa et al., 2025; Priolo et al., 2023; Reijnders et al., 2017; Upadia et al., 2025). Together with the evidence on ARHGEF6 presented here, these studies reinforce the idea that perturbation of the RAC1 regulatory network has major developmental consequences in the human brain.

In conclusion, this study defines a developmental function for ARHGEF6 in forebrain GABAergic INs and provides mechanistic plausibility for how ARHGEF6 dysfunction could contribute to ID and related neurodevelopmental phenotypes. By demonstrating conserved defects in IN migration, maturation, cytoskeletal organization, and survival across mouse and human models, our work strengthens the link between disrupted inhibitory circuit assembly and cognitive impairment and provides experimental support for the relevance of ARHGEF6 dysfunction to human neurodevelopment.

Materials and Methods

Transcriptomic dataset acquisition and processing

The Allen Developing Human Brain Atlas: Developmental Transcriptome dataset, specifically the RNA-Seq Gencode v10 summarized to genes dataset, was downloaded from the Allen Institute for Brain Science (Allen Institute for Brain Science, 2010; available from *brainspan.org*; *RRID:SCR_008083*). Gene expression data were log-normalized using $\log_2$(RPKM + 1). A total of 30 samples from two unique donors were plotted in Figure 1A. The dataset from Wang et al. (2025), entitled Molecular and cellular dynamics of the developing human neocortex, was downloaded from CellxGene. Author-normalized gene expression values were used for this analysis; these values were calculated from raw snRNA-seq counts using SCTransform v2 (0.4.1) (Choudhary & Satija, 2022), as implemented in Seurat v4 (Hao et al., 2021; Wang et al., 2025). The dataset was filtered to include only postnatal data, resulting in the plotting of 114,216 of 232,328 total cells. Eighteen samples from nine unique subjects were plotted. Author-provided cell-type labels were used, and author-generated UMAP coordinates for each cell were obtained from the dataset. Please refer to the original publication for further details on data processing (Wang et al., 2025). Supplementary Table 1 contains postnatal *ARHGEF6* expression values for each cell type. The Mouse Whole Cortex and Hippocampus SMART-Seq dataset, together with the

author-generated UMAP coordinates, was downloaded from the Allen Institute for Brain Science (Yao et al., 2021). This dataset includes scRNA-seq data from approximately 77,000 cells from male and female mice at around 8 weeks of age. Author-generated UMAP coordinates were used. Full names corresponding to acronyms were derived from the original publication and from the whole-mouse brain acronym list provided by the Allen Institute, available at *brain-map.org*. All analyses on this dataset were performed using the trimmed-means gene expression CSV file, in which the data were normalized as $\log_2$(CPM [exons + introns]) before calculation of mean expression for each cell-type cluster. Supplementary Table 2 contains *Arhgef6* expression values for each subclass. Multiple cell clusters were grouped into each subclass, and the trimmed mean expression of each cluster was averaged to obtain mean subclass-level expression. Please refer to the Allen Institute resource for additional information on data processing.

Mouse strains

All animal procedures were approved by the local Animal Ethics Committee and the Ministry of Health. Animals were maintained in accordance with institutional animal welfare guidelines and legislation under veterinary supervision. The *Arhgef6-KO* mouse strain has been previously described (Ramakers et al., 2012) and was obtained from the INTRAFRONTIER EMMA Repository (EM:07499). Heterozygous and homozygous mutant mice are born at normal Mendelian frequency, appear grossly normal, are viable and fertile, mate at normal rates, and do not display evident neurological or motor impairments. Animals were maintained on a mixed C57BL/6 genetic background. The GAD67-eGFP reporter mouse strain has been previously described (DeDiego et al., 1994; Sakai & Miyazaki, 1997; Tamamaki et al., 2003). The progeny resulting from the cross between the reporter strain and the *Arhgef6-KO* strain were healthy and fertile.

Brain preparation for histological analysis

For collection of postnatal brains, mice were anesthetized with Avertin (30 µl of pure Avertin in 400 µl PBS) and transcardially perfused with 10 ml PBS (pH 7.4), followed by 10 ml 4% (w/v) PFA in PBS (pH 7.4, adjusted with NaOH). Brains were dissected, post-fixed overnight at 4°C in 4% PFA, cryoprotected in 30% (w/v) sucrose in PBS followed by 15% (w/v) sucrose in PBS, embedded in OCT, and stored at −80°C until sectioning. OCT blocks were cut into 30 µm-thick coronal sections using a cryostat (Leica CM1950). Free-floating sections were collected in PBS in multiwell plates and stored at −20°C in cryoprotectant solution (30% [v/v] glycerol and 30% [v/v] ethylene glycol in 0.2 M phosphate buffer, pH 7.4) until processing. For collection of embryonic brains, embryos were obtained by cesarean section at E14.5 and E18.5 from anesthetized pregnant dams; detection of a vaginal plug was designated as E0.5. Embryos were transferred into PBS. Embryonic brains used for immunohistochemistry were dissected and fixed overnight at 4°C in 4% PFA, then cryoprotected overnight at 4°C in 30% (w/v) sucrose in PBS, followed by 15% (w/v) sucrose in PBS, embedded in OCT, and stored at −80°C until analysis. OCT blocks were cut into 20 µm-thick coronal sections and collected on adhesive glass slides.

In situ hybridization

The murine *Arhgef6* antisense probe (Lein et al., 2007) was synthesized from adult mouse brain cDNA using the following primers (based on (Lein et al., 2007): forward 5'-CCTCGATTCTCCAGTA ACCATC-3' and reverse 5'-GGCCACTGATGAGTCCAACT-3', with the reverse primer harboring the T7 promoter sequence 5'-GGTAATACGACTCACTATAGGG-3' at the 5' end. Probes were generated by two rounds of 35 PCR cycles using Phusion High-Fidelity DNA Polymerase (New England Biolabs, cat. M0530), followed by in vitro transcription with a digoxigenin (DIG) RNA Labeling Kit (Roche, cat. 11175025910). In situ hybridization was performed on 20 µm coronal cryosections from PFA-fixed wild-type mouse brains at the indicated time points using DIG-labeled antisense riboprobes (2 µg/ml), as previously described (Paganoni et al., 2022). Signal was revealed by colorimetric

staining using 4-nitro blue tetrazolium chloride and 5-bromo-4-chloro-3-indolyl phosphate disodium salt (NBT/BCIP, Roche) in staining solution containing 100 mM NaCl, 50 mM MgCl2, 100 mM Tris-HCl (pH 9.8), 1% Tween 20, and 50% polyvinyl alcohol at 37°C.

Primary cultures of hippocampal neurons

Two-well Ibidi slides were coated with 0.1 mg/ml poly-L-lysine (Sigma) in borate buffer (pH 8.5) and washed with deionized water. One day before establishing the culture, µ-slides were rinsed with MEM (Gibco) supplemented with 1% (v/v) sodium pyruvate 100× (Gibco), 20% (w/v) glucose, 1% (v/v) penicillin-streptomycin, and 10% (v/v) horse serum (Gibco). GAD67-eGFP and GAD67-eGFP;Arhgef6-KO pups at P0 were used to establish primary hippocampal neuronal cultures. Hippocampi were dissected from the brain after removal of the meninges under sterile conditions in a cold solution of 1% (v/v) HEPES in HBSS containing calcium and magnesium (Gibco). Hippocampi were washed in a cold solution containing 1% penicillin-streptomycin and 1% HEPES in HBSS with calcium and magnesium and incubated in 1 ml HBSS containing 25% Trypsin 0.25% (Gibco). Hippocampi were then washed twice in HBSS at 37°C for 10 min each. Tissue was dissociated by pipetting in a solution containing DNase (1:1,000; Promega). Cells were counted, and 430,000 cells were plated in each well containing Neurobasal medium (Gibco) supplemented with 1% penicillin-streptomycin, 2% (v/v) B27 (Gibco), and 0.25% (v/v) GlutaMAX (Gibco). Neurons were maintained at 37°C in a humidified atmosphere containing 5% CO2.

Brain and primary cultures staining

Primary cortical cultures were fixed at 10 days *in vitro* (DIV10) with 4% PFA in PBS for 20 min at room temperature. Neurons were incubated for 1 h at room temperature in a blocking solution containing 5% goat serum and 0.1% Triton X-100 in PBS. The primary antibody (anti-GFP) was diluted in 3% goat serum and 0.1% Triton X-100 in PBS and incubated overnight at 4°C. Secondary antibodies were incubated for 1 h at room temperature. Finally, neurons were counterstained with DAPI before coverslips were mounted with Mowiol onto glass slides. Primary antibody: rabbit anti-GFP. Secondary antibody: Alexa Fluor 488 donkey anti-rabbit IgG (1:500; Invitrogen). Slides were examined with a Leica SP8 confocal microscope. Raw images were digitally processed in ImageJ (NIH, Bethesda, MD, USA) to normalize background, optimize contrast, rotate, and resize images. Morphological analysis of primary cultures was performed in ImageJ; neuronal arborization was quantified by Sholl analysis (Sholl, 1953) using the Sholl Analysis plugin (v1.0; Ghosh Lab Software). Terminal deoxynucleotidyl transferase dUTP nick end labeling (TUNEL; Click-iT™ TUNEL Alexa Fluor Imaging Assays for Microscopy & HCS, Invitrogen) was performed according to the manufacturer's instructions on embryonic brain slices. Before imaging, embryonal sections were counterstained with DAPI and mounted with Mowiol on adhesive glass slides.Stained mouse brain sections were imaged using a 20× objective on a Leica SP8 confocal microscope and used for quantification on ImageJ.

Whole-cell patch-clamp recording

For acute slice recordings, P90 mice were sacrificed by cervical dislocation. Brains were removed quickly and placed in an ice-cold sucrose-based cutting solution containing (in mM): 2.5 KCl, 1.25 NaH_2PO_4, 10 $MgSO_4$, 0.5 $CaCl_2$, 11 glucose, 234 sucrose, and 26 $NaHCO_3$. The solution was continuously bubbled with 95% O_2 / 5% CO_2 to maintain pH 7.3–7.4. Coronal somatosensory cortex slices (300 µm) were cut in ice-cold ACSF using a vibratome (Microm HM650V, Thermo Scientific) and then incubated for 30 min in ACSF containing 119 NaCl, 2.5 KCl, 26 $NaHCO_3$, 2.5 $CaCl_2$, 1.3 $MgSO_4$, 1.2 NaH_2PO_4, and 11 glucose (Liaci et al., 2022; Marcantoni et al., 2014). Slices recovered for 30–45min at 37 °C and then for an additional 1 h at room temperature before recordings. Patch electrodes were fabricated from borosilicate glass (Hilgenberg, Mansfield, Germany) and had a final resistance of 5–9 MΩ. For current-clamp recordings in both brain slices and primary cultured neurons, the internal solution contained 135 mM potassium gluconate, 5 mM NaCl, 2 mM $MgCl_2$, 10 mM HEPES, 0.5 mM EGTA, 2 mM ATP-Tris, and 0.4 mM Tris-GTP. Whole-cell patch-clamp recordings from cortical INs in somatosensory cortex layers IV–VI were

performed using an EPC-10 amplifier (HEKA Elektronik, Lambrecht, Germany). Traces were sampled at 10 kHz and low-pass filtered at 2 kHz with a Bessel filter. All experiments were performed at room temperature (22–24°C). Resting membrane potential (Vrest) and membrane capacitance (C_m) were routinely measured upon establishment of whole-cell configuration. The membrane time constant (τ_m) was calculated in Clampfit following a −30 pA current step injection. Cm was calculated according to $C_m = \tau_m/R_{in}$. Action potential parameters were obtained by analyzing a series of spikes recorded during tonic firing lasting 1–2 min. Tonic firing was elicited by depolarizing the membrane with the minimum current required to reach the rheobase (Marcantoni et al., 2014). After reaching steady-state firing, at least five action potentials were selected and averaged for each cell. Action potential peak amplitude, half-width, maximum rising slope, and maximum repolarizing slope were measured using Clampfit software (Axon Instruments). Peak amplitude was measured from threshold to the action potential peak, and half-width was calculated at half-maximal height. To analyze the relationship between firing frequency and injected current, the membrane potential was adjusted to −70 mV and 20 current pulses of increasing intensity (from −30 to 160 pA; 500 ms duration) were injected. Mean firing frequency at each current step was calculated as the number of spikes per second. Rheobase was defined as the minimum current required to trigger one spike. Input resistance (R_{in}) was calculated from the linear portion of the current-voltage relationship centered at the holding potential (−70 mV), using hyperpolarizing and depolarizing current steps from −30 to 30 pA in 10 pA increments.

hiPSC mutagenesis

Human iPSCs DYS0100 (ATCC) were dissociated using TrypLE Select Enzyme (Gibco) and electroporated using a Lonza 4D-Nucleofector (program CM-113, solution P3) according to the manufacturer's instructions (Umbach et al, 2022). Briefly, equal amounts of 100 µM crRNA and tracrRNA (Integrated DNA Technologies) were mixed and annealed to form gRNAs. A total of 150 pmol gRNA was complexed with 120 pmol Cas9 protein (Integrated DNA Technologies) to form ribonucleoprotein complexes (RNPs). The electroporation mixture was prepared as previously described (Ghetti et al., 2021). After electroporation, cells were plated onto Geltrex-coated plates and maintained in StemFlex medium supplemented with RevitaCell Supplement (Gibco) for 48 h. Monoclonal cell lines were established by single-cell sorting into 96-well plates followed by clonal expansion. Potential off-target sites for gRNA + 4 were analyzed using the Cas-OFFinder online algorithm with the following parameters: SpCas9 from Streptococcus pyogenes (5'-NGG-3'), mismatch number ≤ 4, DNA bulge size = 0, RNA bulge size = 0, and Homo sapiens (GRCh38/hg38) as the target genome. Genomic DNA was extracted using QuickExtract DNA Extraction Solution (Epicentre), and the target locus was amplified by PCR using Phusion High-Fidelity DNA Polymerase (Thermo Fisher). Oligonucleotides used to evaluate indels resulting from cleavage by one crRNA are listed below. Purified PCR products were sequenced and analyzed using Synthego ICE software (Brinkman et al., 2014, 2018; Conant et al., 2022; Kluesner et al., 2018). The following genomic regions were amplified and sequenced to validate CRISPR editing of ARHGEF6 and assess potential off-target effects. Primer sequences, amplicon size, and melting temperature (T_m) are reported below. The target ARHGEF6 locus (chrX:+136747259) was amplified using the forward primer ATCACGAGAACAACTCGGC and the reverse primer GAGTGGGTCTGAGTATGCAC, generating a 480 bp amplicon with a T_m of 58°C. The first predicted off-target site (chrX:+106599275) was amplified using the forward primer GAAATGGTGGTTCCAGACAGC and the reverse primer GAACCGCACCACTCTGTTG, producing a 343 bp amplicon with a T_m of 59°C. The second predicted off-target site (chr6:-67012633) was amplified using the forward primer TCTGTAG CAAAACAACTGGC and the reverse primer TCACCTGCTAATGACCAAACAC, generating a 447 bp amplicon with a T_m of 58.55°C. The third predicted off-target site (chr4:+168553958) was amplified using the forward primer TGAACACCCATTGCATCCCCTC and the reverse primer AGGTGCCCAGAAG ACCTTTATC, producing a 640 bp amplicon with a T_m of 59.16°C.

hiPSC differentiation into neural progenitors and embryoid bodies

Human iPSCs (hiPSCs) were expanded on Geltrex-coated 6-well plates in Essential 8 (E8; Gibco) medium, which was changed daily. For passaging, cultures were washed with DPBS and exposed to 0.5 mM EDTA dissociation solution at 37°C until the cells and colonies appeared rounded but not fully detached. The dissociation buffer was then removed, colonies were collected and transferred to a 15 ml Falcon tube, centrifuged at 200 × g for 5 min, resuspended in E8 medium, and replated in 6-well plates. Cells were maintained at 37°C in 5% CO2, and medium was replaced daily. For embryoid body (EB) formation, hiPSCs were collected from one well of a 6-well plate at 70–80% confluence, centrifuged at 200 × g for 5 min, and the pellet was gently resuspended in complete E8 medium. Cells from each clone were plated in 4 ml complete E8 medium supplemented with 5 µM ROCK inhibitor Y-27632 into a 6-well plate pretreated with Pluronic acid. Plates were coated with 50 mg/ml Pluronic acid solution for 1 h at room temperature. The plate was gently tilted several times to distribute the cell suspension evenly, and cells were cultured under standard conditions (37°C, 5% CO2, 21% O2). EBs were checked daily, and medium was replaced every second day. During medium changes, EBs were collected into a 15 ml Falcon tube, allowed to settle by gravity, the supernatant was replaced, and the EBs were returned to the original wells. From day 2 to day 7, cultures were gradually shifted from E8 medium to Essential 6 (E6; Gibco) medium until EBs were maintained exclusively in E6. On day 7, EBs were transferred onto Geltrex-coated µ-Slide 2-well Ibidi chambers to allow adhesion and imaging analysis. E6 medium was replaced every other day. Neural induction, corresponding to the conversion of human iPSCs into neural progenitor cells (NPCs), was performed using PSC Neural Induction Medium (Gibco) according to the manufacturer's instructions.

hiPSC and hiPSC-derived cell staining

Cells plated in Geltrex-coated µ-Slide 2-well Ibidi chambers were fixed with 4% PFA for 30 min at room temperature and washed with PBS before incubation for 1 h in PBS containing 0.3% Triton X-100 (Sigma, T9284) and 6% BSA (Sigma, AA0281). Cells were incubated overnight at 4°C with primary antibodies, followed by incubation for 2 h at room temperature with secondary antibodies; both antibody solutions consisted of PBS containing 0.1% Triton X-100 and 2.5% BSA, with three washes before and after secondary antibody incubation. Primary antibodies used were mouse anti-OCT3/4 (1:1,000; Santa Cruz Biotechnology, sc-5279), rabbit anti-SOX2 (1:1,000; Abcam, AB97959), mouse anti-GATA4 (1:1,000; Santa Cruz Biotechnology, sc-25310), rabbit anti-TUJ1 (1:1,000; GeneTex, GTX130245), mouse anti-ACTA2 (1:1,000; Antibodies, A279072), mouse anti-NESTIN (1:1,000; R&D Systems, MAB1259), mouse anti-PAX6 (1:1,000; BD Pharmingen, 561462), and rabbit anti-FABP7 (Millipore, ABN14). For phalloidin staining, cells were washed in PBS and fixed in 4% formaldehyde in PBS for 30 min. Cells were permeabilized with 0.1% Triton X-100 in PBS for 5 min and blocked in 3% non-fat dry milk in PBS for 30 min. A total of 200 µl Phalloidin-FITC (1:500 in BSA 10× PBS) was added to each well for 90 min. Mowiol was used as mounting medium to preserve fluorescence. Coverslips were examined with a Leica SP8 laser scanning confocal microscope using 488 nm excitation. Images were analyzed in ImageJ software for corrected total cell fluorescence (CTCF), calculated from integrated density and background fluorescence measurements. Single rosettes were imaged for 14 h under bright-field illumination using a 20× objective on a Leica Thunder Microscope. Temperature and CO2 were maintained at 37°C and 5%, respectively, throughout the recording. Anisotropy was automatically calculated using the FibrilTool plugin in ImageJ (Boudaoud et al., 2014).

Differentiation and assembly of dorsal and ventral organoids

Cortical and ventral differentiations from hiPSCs were performed as previously described (Birey et al., 2017; Sloan et al., 2018). For feeder-free cortical and ventral differentiation, hiPSCs were maintained on Geltrex-coated Costar plates in Essential 8 medium in a humidified atmosphere containing 5% CO2. Cells were passaged every 4–5 days using UltraPure 0.5 mM EDTA, pH 8.0 (Thermo Fisher Scientific, 15575020). On day 0, feeder-free human pluripotent stem cells at 80–90% confluence were dissociated into single cells with Accutase and reaggregated at 9,000 cells per

well in ultra-low-attachment 96-well V-bottom plates (sBio PrimeSurface plate; Sumitomo Bakelite) in Essential 6 medium supplemented with the SMAD pathway inhibitors dorsomorphin (2.5 mM, Sigma-Aldrich, P5499) and SB431542 (10 mM, R&D Systems, 1614). Feeder-free cortical differentiation was performed as previously described (Yoon et al., 2019) using the protocol variant without XAV939. Feeder-free ventral differentiation was based on the feeder-free cortical protocol with the following additional treatments: XAV-939 (2.5 mM, Tocris, 3748) from day 3 to day 6; IWP-2 (2.5 mM, Selleck Chemicals, S7085) from day 7 to day 24; and SAG (100 nM, EMD Millipore, 566660) from day 13 to day 24. To promote progenitor differentiation, BDNF (20 ng/ml) and NT-3 (20 ng/ml) were added starting on day 25, with medium changes every other day. After day 43, medium was changed every 4–5 days using neural medium without growth factors. Assembly of cortical and ventral organoids to generate forebrain assembloids was performed as previously described (Birey et al., 2017; Sloan et al., 2018). 2-month-old ventral organoids were transduced with DLX1/2b-eGFP lentivirus (gift from S. Pasca and J. Rubenstein) as described in Paulsen et al. (2022). Bright-field images of all organoids were acquired from day 3 to day 60. ImageJ software was used to measure the area and perimeter of each organoid, and Prism software was used to plot the average size of organoids for each differentiation condition.

Organoid IN morphological analysis

4-month-old ventral forebrain organoids transduced with DLX1/2b-eGFP lentivirus were imaged using a 25× water immersion objective on a Leica SP8 two-photon microscope. The SNT Neuroanatomy plugin (Arshadi et al., 2021) in ImageJ was used to perform Sholl analysis (Sholl, 1953).

Organoid staining

Organoids were fixed with 4% PFA for 30 min at room temperature and then incubated overnight at 4°C in 30% sucrose solution. Organoids were embedded in Tissue-Tek O.C.T. compound (Sakura, 62550) and sectioned at 25 µm with a cryostat onto glass slides (Globe Scientific, 1354W). Slides were washed three times in PBS containing 0.1% Tween-20 (Sigma, P9416), then incubated for 1 h in PBS containing 0.3% Triton X-100 (Sigma, T9284) and 6% BSA (Sigma, AA0281). Slides were incubated overnight at 4°C with primary antibodies, followed by incubation for 2 h at room temperature with secondary antibodies. Both antibody solutions consisted of PBS containing 0.1% Triton X-100 and 2.5% BSA, with three washes before and after secondary antibody incubation. Slides were coverslipped using Fluoromount-G (EMS, 50-259-73). Primary antibodies used were goat anti-SOX2 (1:1,000; R&D Systems, AF2018), rabbit anti-NKX2.1 (1:500; Abcam, ab76013), rabbit anti-NEUN (1:200; Abcam, ab177487), mouse anti-SATB2 (1:100; Abcam, ab51502). TUNEL staining was performed according to the manufacturer's instructions. Stained organoids were imaged using a 10× objective on a Leica Thunder Microscope and used for quantification.

Organoids live imaging and analysis

Migration analysis. Live imaging of forebrain assembloids, whose ventral compartment had been previously transduced with LV-DLX1/2b-eGFP lentivirus, was performed using a 10× objective on a Leica THUNDER microscope, following the protocol described by Birey et al. (2017). All analyses were performed in ImageJ. Individual neurons were modeled as polylines defined by three points (A, B, and C), yielding two segments: AB, extending from the rear to the front of the soma, and BC, extending from the front of the soma to the tip of the leading process. A saltation event was defined as a sequence in which elongation of the total neuronal length, approximated as AB + BC, was followed by shortening.

Growth cone analysis. Approximately 1-month-old forebrain organoids were transduced with LifeAct-GFP lentivirus (Addgene, 51010), followed by a medium change 24 h after transduction. Five days after transduction, organoids were individually transferred to 1:70 Geltrex-coated µ-Slide 8-well glass-bottom plates (Ibidi, 80827). A volume of 1.5 µl Geltrex was applied directly to each organoid to promote attachment. To visualize growth cone dynamics in neurons extending processes outside the organoids, live imaging was performed over the following 10 days using a

63× oil immersion objective on a Leica Thunder Microscope. Time-lapse images were acquired in the GFP channel every 5 min for a total imaging period of 250 min for each selected field. Temperature and CO_2 were maintained at 37°C and 5%, respectively, throughout the recording using a live-imaging chamber. Growth cones were manually selected for size and morphological analysis in ImageJ. The average rate of change in size was computed as the relative change between consecutive time points, $(S_{t+1}-S_t)/S_t$, summed across the time series and normalized to the total imaging duration (250”).

Statistical analysis

Statistical analyses were performed using GraphPad Prism (GraphPad Software Inc.). The statistical test used for each experiment is indicated in the corresponding figure legends. Shapiro-Wilk and Kolmogorov-Smirnov tests were used to assess normality, and the F test was used to assess equality of variance; these results were used to select the appropriate statistical test. Data are presented as the mean ± standard error of the mean (SEM). In violin plots, the width of the violin reflects the distribution density of the data, the central line indicates the median, and the flanking lines indicate the interquartile range. Statistical significance was set at $p < 0.05$.

Figure supplements

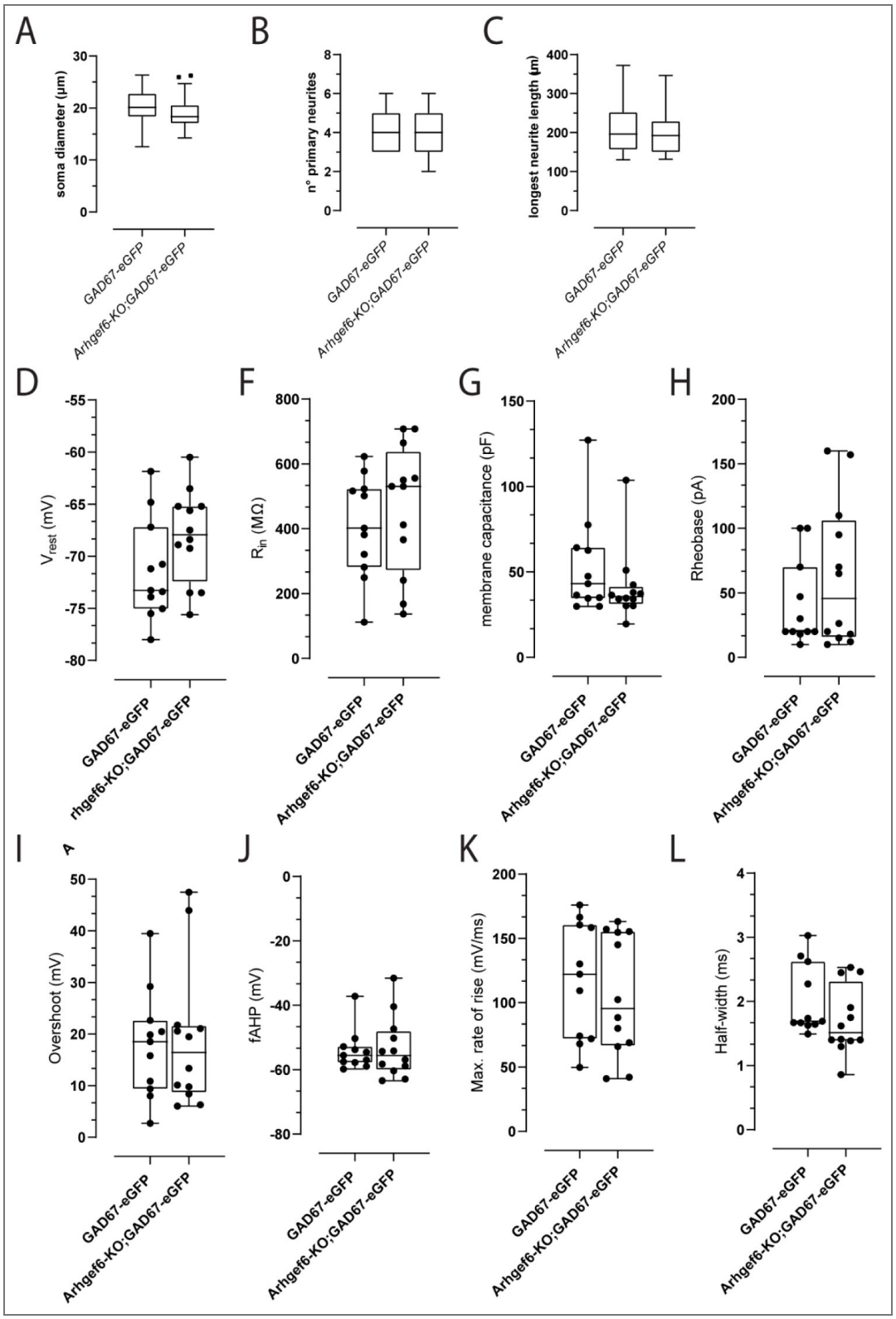

Supplementary Figure 1. Morphological and intrinsic electrophysiological properties of *GAD67-eGFP* and *GAD67-eGFP;Arhgef6-KO* INs. A–C. Quantification of morphological parameters of reconstructed hippocampal primary INs after 10 days *in vitro* (DIV). p-values = 0.055 (soma diameter), 0.76 (number of primary neurites), 0.385 (longest neurite length). **D–H**. Passive membrane properties measured by whole-cell patch-clamp recordings in

eGFP$^+$ INs from control and *Arhgef6-KO* cultures. p-values = 0.105 (resting membrane potential, V_{rest}), 0.464 (input resistance, R_{in}), 0.287 (membrane capacitance), 0.275 (rheobase). **I–L**. Active membrane properties of recorded INs. p-values = 0.829 (action potential overshoot), 0.928 (after-hyperpolarization amplitude, AHP), 0.553 (maximum rate of rise of the action potential, Max. rate of rise), 0.182 (action potential half-width). p-values were calculated using unpaired t-test (F-I, K,L) and Mann-Whitney test (A-C, D, J). * = p< 0.05, ** = p< 0.01, *** = p< 0.001. Data are presented as mean ± SEM. Each dot represents an individual recorded neuron; box plots show median and interquartile range with whiskers indicating the data range.

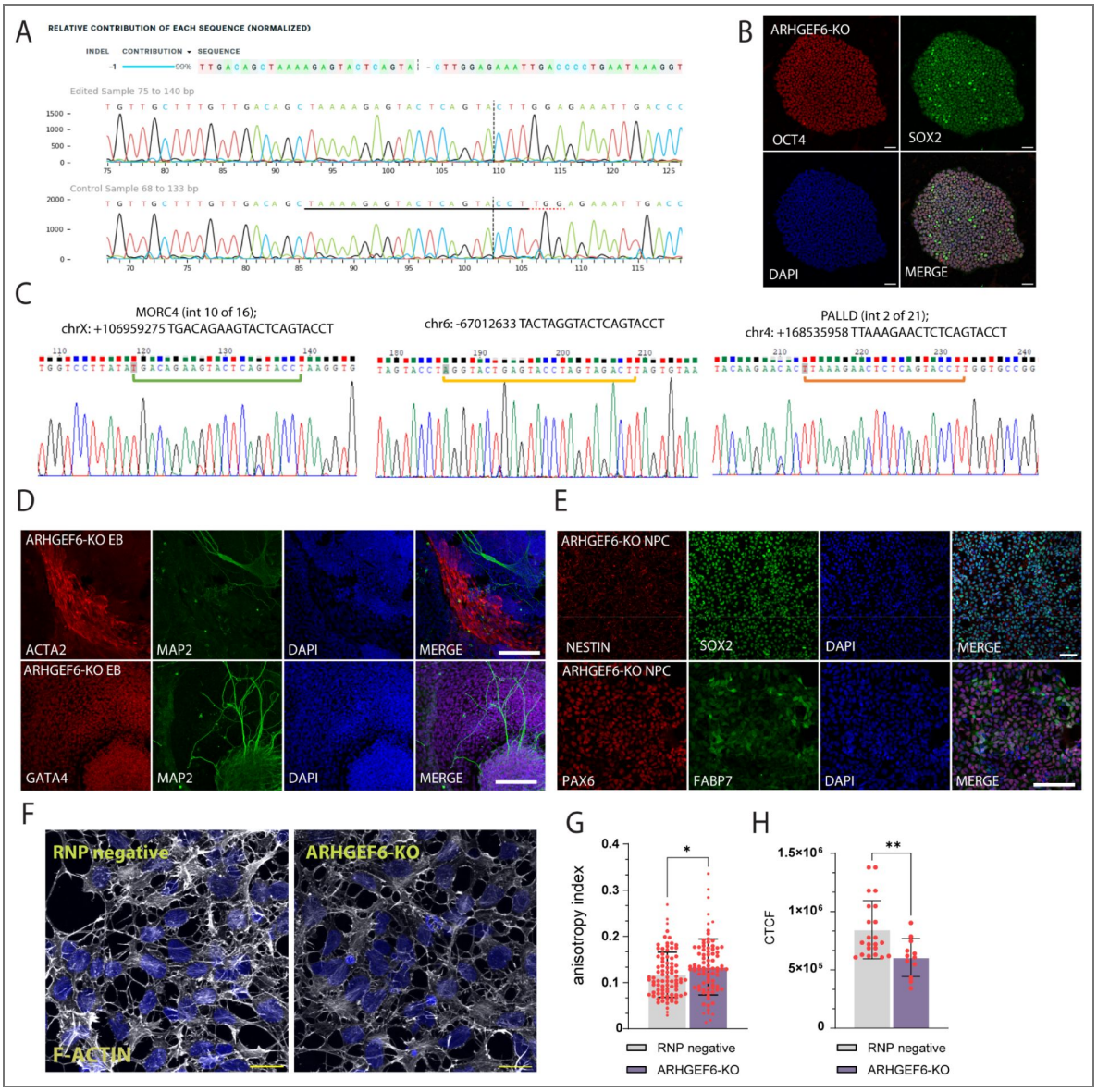

Supplementary Figure 2. Mutagenesis of *ARHGEF6* in hiPSC and characterization of the line.

A. Chromatogram of Sanger sequencing of human induced pluripotent stem cells (hiPSCs) ATCC-DYS0100, edited clone *ARHGEF6-KO* (top) and RNP negative isogenic control (bottom). The dashed line indicates the site of the CRISPR/Cas9 double-strand break. The mutation resulted in the deletion of a single cytosine, causing a frameshift mutation. **B**. Immunofluorescence staining for the expression of hiPSCs markers OCT4 (red) and SOX2 (green) in *ARHGEF6-KO* iPSCs. Nuclei were stained with DAPI (blue). Scale bars, 50 µm. **C**. Chromatograms from Sanger sequencing of the edited hiPSC clone showing no sequence changes at the top 3 predicted crRNA off-target sites. **D**. Immunofluorescence staining of marker genes for all three germ layers in embryoid bodies (EBs) obtained from *ARHGEF6-KO* hiPSCs. ACTA2 (mesoderm derivative, top, red), TUJ1/MAP2 (neuroectoderm, green), GATA4 (endoderm, bottom, red) and nuclei were stained with DAPI (blue). Scale bars, 200 µm. **E**. Immunofluorescence staining of neuroepithelial markers (top) Nestin (red), SOX2 (green), and radial glia markers (bottom) PAX6 (red) and FABP7 (green) in neural progenitor cells (NPCs) obtained from *ARHGEF6-KO* hiPSCs. Scale bars, 80 µm, 200 µm. **F**. Phalloidin-FITC staining of NPCs obtained from RNP negative (control) and *ARHGEF6*-KO hiPSC. Scale bars, 50 µm. **G**. Quantification of the anisotropy of F-Actin fibers in NPCs stained with Phalloidin-FITC. p-value = 0.0464. **H**. Quantification of polymerized F-actin by measuring the corrected total cell fluorescence (CTCF) of Phalloidin–FITC staining. p-value = 0.0056. p-values were calculated using unpaired t-test. * = p< 0.05, ** = p< 0.01, *** = p< 0.001. Data are presented as mean ± SEM. Each dot corresponds to a cell derived from 3 distinct batches of differentiation.

Data availability

The raw data supporting the conclusion of this article will be made available by the authors without undue reservation.

Acknowledgements

We thank Dr. Seth Ruffis (Optical Imaging Facility, Eli and Edythe Broad CIRM Center for Regenerative Medicine and Stem Cell Research, University of Southern California) and Dr. Marta Gai (Open Lab of Advanced Microscopy, OLMA@MBC, Molecular Biotechnology Center "Guido Tarone," Università di Torino), and Federica Antico (Molecular Biotechnology Center "Guido Tarone," Università di Torino) for their technical assistance. We thank Dr. S. Pasca and Dr. J. Rubenstein for generously providing the DLX1/2b-eGFP lentiviral vector. This work was also supported by Department of Excellence funding from the Italian Ministry of University and Research (MUR) for the 2023–2027 period, awarded to the Department of Neurosciences 'Rita Levi Montalcini' at the University of Turin.

Additional information

Ethics statement

The animal study was reviewed and approved by the Italian Ministry of Health.

Contributions

C.L., G.R.M., L.C., and G.Q. conceived the experiments. C.L., B.S., E.F., J.P.U., J.J.L., G.C., L.P., M.C., R.M., S.R., A.U., E.H., G.C., R.O., A.P., and V.T. performed the experiments. A.M., M.G., A.C., and L.C. provided materials and tools. C.L., G.R.M., and G.Q. supervised all aspects of the project. C.L., G.R.M., and G.Q. wrote the manuscript and designed the figures.

Funding

This work was supported by the Italian Telethon Foundation (GGP20039 to G.R.M.), the Italian Ministry of University and Research (MUR; PRIN 2023 to G.R.M.), and the National Institutes of Health (NIH; R01MH136351 and R01MH138371 to G.Q.). C.L. was supported by the Italian Society of Biophysics and Molecular Biology (SIBBM) in 2024. A.P. was supported by Fondazione Veronesi (Italy).

Funding

Funder	Grant reference number	Author
Fondazione Telethon (FT)	GGP20039	Giorgio Roberto Merlo
Italian Ministry of University and Research	PRIN 2023	Giorgio Roberto Merlo
HHS | National Institutes of Health (NIH)	R01MH136351	Giorgia Quadrato
HHS | National Institutes of Health (NIH)	R01MH138371	Giorgia Quadrato
Italian Society of Biophysics and Molecular Biology (SIBBM)	2024	Carla Liaci
Fondazione Veronesi		Alyssa Paganoni

Author ORCID iDs

Carla Liaci: https://orcid.org/0000-0003-4508-516X
Mattia Camera: https://orcid.org/0000-0003-4257-0629
Maurizio Giustetto: https://orcid.org/0000-0003-1323-4060

Giorgio R Merlo: https://orcid.org/0000-0002-6478-0486

Additional files

Supplementary Table 1. Human postnatal *ARHGEF6* expression by cell type. Single-nucleus RNA-sequencing (snRNA-seq) data from human postnatal donors (3 months - 13 years). Full snapshot of data used in Fig. 1B. Mean *ARHGEF6* expression per cell type across each postnatal timepoint and including all postnatal timepoints. Postnatal expression range: 0.0000 – 3.0445. 114,216 cells included from 18 samples across 9 unique subjects. 9,010 / 114,216 (7.9%) cells expressed *ARHGEF6* > 0. NaN occurs in the table when no cells of that cell type were present at the timepoint. EN-IT-Immature, intratelencephalic excitatory immature neurons; EN-L2_3-IT, layer 2/3 intratelencephalic excitatory neurons; EN-L4-IT, layer 4 intratelencephalic excitatory neurons; EN-L5-ET, layer 5 extratelencephalic excitatory neurons; EN-L5-IT, layer 5 intratelencephalic excitatory neurons; EN-L5_6-NP, layer 5/6 near-projecting excitatory neurons; EN-L6-CT, layer 6 corticothalamic excitatory neurons; EN-L6-IT, layer 6 intratelencephalic excitatory neurons; EN-L6b, layer 6b excitatory neurons; EN-Newborn, Newborn excitatory neurons; EN-Non-IT-Immature, immature non-intratelencephalic excitatory neuron;. IN-CGE-Immature, immature caudal ganglionic eminence-derived inhibitory neurons; IN-CGE-SNCG, immature caudal ganglionic eminence-derived gamma-synuclein inhibitory neurons; IN-CGE-VIP, caudal ganglionic eminence-derived vasoactive intestinal polypeptide inhibitory neurons; IN-MGE-Immature, immature medial ganglionic eminence-derived inhibitory neurons; IN-MGE-PV, medial ganglionic eminence-derived parvalbumin inhibitory neurons; IN-MGE-SST, medial ganglionic eminence-derived somatostatin inhibitory neurons; IN-Mix-LAMP5, mixed lysosomal-associated membrane protein family member 5 inhibitory neurons; IN-NCx_dGE-Immature, immature neocortex and dorsal ganglionic eminence-derived inhibitory neurons; IPC-EN, intermediate progenitor cell for excitatory neurons; OPC, oligodendrocyte precursor cells; RG-oRG, outer radial glial cells; RG-tRG, truncated radial glial cells; RG-vRG, ventricular radial glial cells; Tri-IPC, tripotential intermediate progenitor cells.

Supplementary Table 2. Adult mouse *Arhgef6* expression values by cell subclass. Single-cell RNA-sequencing (scRNA-seq) data from ~8 week old (~P56) mice. Multiple cell clusters were grouped into each subclass, and the trimmed mean expression of each cluster was utilized to calculate subclass-level expression statistics. 73347 cells included. PV, parvalbumin; SST, somatostatin; SST CHOLD, somatostatin and chondrolectin; LAMP5, lysosomal-associated membrane protein family member 5; SNCG, gamma-synuclein; VIP, vasoactive intestinal polypeptide; MEIS2, meis homeobox 2; CR, cajal-retzius cell; L2 IT ENTl, layer 2 intratelencephalic lateral entorhinal area; L2 IT ENTm, layer 2 intratelencephalic medial entorhinal area; L2/3 IT CTX, layer 2/3 intratelencephalic isocortex; L2/3 IT ENTl, layer 2/3 intratelencephalic lateral entorhinal area; L2/3 IT PPP, layer 2/3 intratelencephalic postsubiculum-presubiculum-parasubiculum; L2/3 IT RHP, layer 2/3 intratelencephalic retrohippocampal region; L3 IT ENT, layer 3 intratelencephalic entorhinal area; L4 RSP-ACA, layer 4 retrosplenial area-anterior cingulate area; L4/5 IT CTX, layer 4/5 intratelencephalic isocortex; L5 IT CTX, layer 5 intratelencephalic isocortex; L5 PPP, layer 5 postsubiculum-presubiculum-parasubiculum; L5 PT CTX, layer 5 pyramidal tract isocortex; L5/6 IT TPE-ENT, layer 5/6 intratelencephalic temporal association areas-perirhinal area-ectorhinal area-entorhinal area; L5/6 NP CTX, layer 5/6 near-projecting isocortex; L6 CT CTX, layer 6 corticothalamic isocortex; L6 IT CTX, layer 6 intratelencephalic isocortex; L6 IT ENTl, layer 6 intratelencephalic lateral entorhinal area; L6b CTX, layer 6b isocortex; L6b/CT ENT, layer 6b corticothalamic entorhinal area; NP PPP, near-projecting postsubiculum-presubiculum-parasubiculum; NP SUB, near-projecting subiculum; CT SUB, corticothalamic subiculum; Car3, carbonic anhydrase 3; SUB-Pros, subiculum-prosubiculum; CA1-ProS, field cornu ammonis 1-prosubiculum; CA2-IG-FC, field cornu ammonis 2-fasciola cinerea-indusium griseum; CA3, field cornu ammonis 3; DG, dentate gyrus; Astro, astrocyte; Oligo, oligodendrocyte; Micro-PVM, microglia/perivascular macrophage; Endo, endothelial cell; SMC-Peri, smooth muscle cell perivascular area; VLMC, vascular leptomeningeal cell.

Supplementary Video 1. Representative time-lapse imaging of migrating RNP negative DLX1/2b-eGFP+ INs in fused assembloids.

Supplementary Video 2. Representative time-lapse imaging of migrating *ARHGEF6-KO* DLX1/2b-eGFP+ INs in fused assembloids.

Supplementary Video 3. Representative time-lapse imaging of an RNP negative LifeAct-GFP+ growth cone.

Supplementary Video 4. Representative time-lapse imaging of an *ARHGEF6-KO* LifeAct-GFP^{+} growth cone.

References

Aerts T., Seuntjens E (2021) Novel perspectives on the development of the amygdala in rodents. *Frontiers in Neuroanatomy* **15**:786679 https://doi.org/10.3389/fnana.2021.786679 | PubMed

Arshadi C., Günther U., Eddison M., Harrington K. I. S., Ferreira T. A (2021) SNT: A unifying toolbox for quantification of neuronal anatomy. *Nature Methods* **18**:374-377 https://doi.org/10.1038/s41592-021-01105-7 | PubMed

Bagley J. A., Reumann D., Bian S., Lévi-Strauss J., Knoblich J. A (2017) Fused cerebral organoids model interactions between brain regions. *Nature Methods* **14**:743-751 https://doi.org/10.1038/nmeth.4304 | PubMed

Banka S., Bennington A., Baker M. J., Rijckmans E., Clemente G. D., Ansor N. M., Sito H., Prasad P., Anyane-Yeboa K., Badalato L., *et al.* (2022) Activating RAC1 variants in the switch II region cause a developmental syndrome and alter neuronal morphology. *Brain* **145**:4232-4245 https://doi.org/10.1093/brain/awac049 | PubMed

Birey F., Andersen J., Makinson C. D., Islam S., Wei W., Huber N., Fan H. C., Metzler K. R. C., Panagiotakos G., Thom N., *et al.* (2017) Assembly of functionally integrated human forebrain spheroids. *Nature* **545**:54-59 https://doi.org/10.1038/nature22330 | PubMed

Birey F., Pașca S. P. (2022) Imaging neuronal migration and network activity in human forebrain assembloids. *STAR Protocols* **3**:101478 https://doi.org/10.1016/j.xpro.2022.101478 | PubMed

Bitzenhofer S. H., Pöpplau J. A., Chini M., Marquardt A., Hanganu-Opatz I. L (2021) A transient developmental increase in prefrontal activity alters network maturation and causes cognitive dysfunction in adult mice. *Neuron* **109**:1350-1364.e6 https://doi.org/10.1016/j.neuron.2021.02.011 | PubMed

Blanquie O., Kilb W., Sinning A., Luhmann H. J (2017) Homeostatic interplay between electrical activity and neuronal apoptosis in the developing neocortex. *Neuroscience* **358**:190-200 https://doi.org/10.1016/j.neuroscience.2017.06.030 | PubMed

Bonifazi P., Goldin M., Picardo M. A., Jorquera I., Cattani A., Bianconi G., Represa A., Ben-Ari Y., Cossart R (2009) GABAergic hub neurons orchestrate synchrony in developing hippocampal networks. *Science* **326**:1419-1424 https://doi.org/10.1126/science.1175509 | PubMed

Boudaoud A., Burian A., Borowska-Wykręt D., Uyttewaal M., Wrzalik R., Kwiatkowska D., Hamant O (2014) FibrilTool, an ImageJ plug-in to quantify fibrillar structures in raw microscopy images. *Nature Protocols* **9**:457-463 https://doi.org/10.1038/nprot.2014.024 | PubMed

Brinkman E. K., Chen T., Amendola M., van Steensel B. (2014) Easy quantitative assessment of genome editing by sequence trace decomposition. *Nucleic Acids Research* **42**:e168 https://doi.org/10.1093/nar/gku936 | PubMed

Brinkman E. K., Chen T., de Haas M., Holland H. A., Akhtar W., van Steensel B. (2018) Kinetics and fidelity of the repair of Cas9-induced double-strand DNA breaks. *Molecular Cell* **70**:801-813.e6 https://doi.org/10.1016/j.molcel.2018.04.016 | PubMed

Cai Y., Zhao Z., Shi M., Zheng M., Gong L., He M (2024) Embryonic origins of forebrain oligodendrocytes revisited by combinatorial genetic fate mapping. *eLife* **13**:RP95406 https://doi.org/10.7554/eLife.95406 | PubMed

Causeret F., Coppola E., Pierani A (2018) Cortical developmental death: Selected to survive or fated to die. *Current Opinion in Neurobiology* **53**:35-42 https://doi.org/10.1016/j.conb.2018.04.022 | PubMed

Chen L., Liao G., Waclaw R. R., Burns K. A., Linquist D., Campbell K., Zheng Y., Kuan C. Y (2007) Rac1 controls the formation of midline commissures and the competency of tangential migration in ventral telencephalic neurons. *The Journal of neuroscience: the official journal of the Society for Neuroscience* **27**:3884-3893 https://doi.org/10.1523/jneurosci.3509-06.2007 | PubMed

Chen L., Melendez J., Campbell K., Kuan C. Y., Zheng Y (2009) Rac1 deficiency in the forebrain results in neural progenitor reduction and microcephaly. *Developmental Biology* **325**:162-170 https://doi.org/10.1016/j.ydbio.2008.10.023 | PubMed

Choudhary S., Satija R (2022) Comparison and evaluation of statistical error models for scRNA-seq. *Genome Biology* **23**:27 https://doi.org/10.1186/s13059-021-02584-9 | PubMed

Conant D., Hsiau T., Rossi N., Oki J., Maures T., Waite K., Yang J., Joshi S., Kelso R., Holden K., *et al.* (2022) Inference of CRISPR edits from Sanger trace data. *The CRISPR Journal* **5**:123-130 https://doi.org/10.1089/crispr.2021.0113 | PubMed

DeDiego I., Smith-Fernández A., Fairén A (1994) Cortical cells that migrate beyond area boundaries: Characterization of an early neuronal population in the lower intermediate zone of prenatal rats. *The European Journal of Neuroscience* **6**:983-997 https://doi.org/10.1111/j.1460-9568.1994.tb00593.x | PubMed

Duerinckx S., Abramowicz M (2018) The genetics of congenitally small brains. *Seminars in Cell & Developmental Biology* **76**:76-85 https://doi.org/10.1016/j.semcdb.2017.09.015 | PubMed

Eid L., Lokmane L., Raju P. K., Tene Tadoum S. B., Jiang X., Toulouse K., Lupien-Meilleur A., Charron-Ligez F., Toumi A., Backer S., *et al.* (2025) Both GEF domains of the autism and developmental epileptic encephalopathy-associated Trio protein are required for proper tangential migration of GABAergic interneurons. *Molecular Psychiatry* **30**:1338-1358 https://doi.org/10.1038/s41380-024-02742-y | PubMed

Govek E. E., Hatten M. E., Van Aelst L. (2011) The role of Rho GTPase proteins in CNS neuronal migration. *Developmental Neurobiology* **71**:528-553 https://doi.org/10.1002/dneu.20850 | PubMed

Ghetti S., Burigotto M., Mattivi A., Magnani G., Casini A., Bianchi A., Cereseto A., Fava L. L (2021) CRISPR/Cas9 ribonucleoprotein-mediated knockin generation in hTERT-RPE1 cells. *STAR Protocols* **2**:100407 https://doi.org/10.1016/j.xpro.2021.100407 | PubMed

Gupta N (2023) Deciphering intellectual disability. *Indian Journal of Pediatrics* **90**:160-167 https://doi.org/10.1007/s12098-022-04345-3 | PubMed

Hansen D. V., Lui J. H., Flandin P., Yoshikawa K., Rubenstein J. L., Alvarez-Buylla A., Kriegstein A. R (2013) Non-epithelial stem cells and cortical interneuron production in the human ganglionic eminences. *Nature Neuroscience* **16**:1576-1587 https://doi.org/10.1038/nn.3541 | PubMed

Hao Y., Hao S., Andersen-Nissen E., Mauck W. M, Zheng S., Butler A., Lee M. J., Wilk A. J., Darby C., Zager M., *et al.* (2021) Integrated analysis of multimodal single-cell data. *Cell* **184**:3573-3587.e29 https://doi.org/10.1016/j.cell.2021.04.048 | PubMed

Hass Y, Kniep J, Hoffrichter A, Marsoner F, Eşiyok N, Gasparotto M, Xing L, Loco Detto Gava MP, Artioli A, Guida C, *et al.* (2025) ARHGAP11A maintains cortical progenitor identity through RHOA-ROCK signaling during human brain development. *Cell Reports* **44**:116599 https://doi.org/10.1016/j.celrep.2025.116599 | PubMed

Heck N., Golbs A., Riedemann T., Sun J. J., Lessmann V., Luhmann H. J (2008) Activity-dependent regulation of neuronal apoptosis in neonatal mouse cerebral cortex. *Cerebral Cortex* **18**:1335-1349 https://doi.org/10.1093/cercor/bhm165 | PubMed

Haugh I. M., Pineider J. L., Agim N. G (2021) Ichthyosiform changes in a patient with RAC1 mutation. *Pediatric Dermatology* **38**:1590-1591 https://doi.org/10.1111/pde.14844 | PubMed

Isaacson J. S., Scanziani M (2011) How inhibition shapes cortical activity. *Neuron* **72**:231-243 https://doi.org/10.1016/j.neuron.2011.09.027 | PubMed

Jaffe A. B., Hall A (2005) Rho GTPases: Biochemistry and biology. *Annual Review of Cell and Developmental Biology* **21**:247-269 https://doi.org/10.1146/annurev.cellbio.21.020604.150721 | PubMed

Keefe F., Monzón-Sandoval J., Rosser A. E., Webber C., Li M (2023) Single-cell transcriptomics reveals conserved regulatory networks in human and mouse interneuron development. *International Journal of Molecular Sciences* **24**:8122 https://doi.org/10.3390/ijms24098122 | PubMed

Kirmse K., Zhang C (2022) Principles of GABAergic signaling in developing cortical network dynamics. *Cell Reports* **38**:110568 https://doi.org/10.1016/j.celrep.2022.110568 | PubMed

Kluesner M. G., Nedveck D. A., Lahr W. S., Garbe J. R., Abrahante J. E., Webber B. R., Moriarity B. S (2018) EditR: A method to quantify base editing from Sanger sequencing. *The CRISPR Journal* **1**:239-250 https://doi.org/10.1089/crispr.2018.0014 | PubMed

Kutsche K., Yntema H., Brandt A., Jantke I., Nothwang H. G., Orth U., Boavida M. G., David D., Chelly J., Fryns J. P., *et al.* (2000) Mutations in ARHGEF6, encoding a guanine nucleotide exchange factor for Rho GTPases, in patients with X-linked mental retardation. *Nature Genetics* **26**:247-250 https://doi.org/10.1038/80002 | PubMed

Lein E. S., Hawrylycz M. J., Ao N., Ayres M., Bensinger A., Bernard A., Boe A. F., Boguski M. S., Brockway K. S., Byrnes E. J., *et al.* (2007) Genome-wide atlas of gene expression in the adult mouse brain. *Nature* **445**:168-176 https://doi.org/10.1038/nature05453 | PubMed

Liaci C., Camera M., Caslini G., Rando S., Contino S., Romano V., Merlo G. R (2021) Neuronal cytoskeleton in intellectual disability: From systems biology and modeling to therapeutic opportunities. *International Journal of Molecular Sciences* **22**:6167 https://doi.org/10.3390/ijms22116167 | PubMed

Liaci C., Camera M., Zamboni V., Sarò G., Ammoni A., Parmigiani E., Ponzoni L., Hidisoglu E., Chiantia G., Marcantoni A., *et al.* (2022) Loss of ARHGAP15 affects the directional control of migrating interneurons in the embryonic cortex and increases susceptibility to epilepsy. *Frontiers in Cell and Developmental Biology* **10**:875468 https://doi.org/10.3389/fcell.2022.875468 | PubMed

Lian G., Wong T., Lu J., Hu J., Zhang J., Sheen V (2019) Cytoskeletal associated Filamin A and RhoA affect neural progenitor specification during mitosis. *Cerebral Cortex* **29**:1280-1290 https://doi.org/10.1093/cercor/bhy033 | PubMed

Lim L., Mi D., Llorca A., Marín O (2018) Development and functional diversification of cortical interneurons. *Neuron* **100**:294-313 https://doi.org/10.1016/j.neuron.2018.10.009 | PubMed

Ma T., Wang C., Wang L., Zhou X., Tian M., Zhang Q., Zhang Y., Li J., Liu Z., Cai Y., *et al.* (2013) Subcortical origins of human and monkey neocortical interneurons. *Nature Neuroscience* **16**:1588-1597 https://doi.org/10.1038/nn.3536 | PubMed

Maia N., Nabais Sá M. J., Melo-Pires M., de Brouwer A. P. M., Jorge P. (2021) Intellectual disability genomics: Current state, pitfalls and future challenges. *BMC Genomics* **22**:909 https://doi.org/10.1186/s12864-021-08227-4 | PubMed

Manser E., Loo T. H., Koh C. G., Zhao Z. S., Chen X. Q., Tan L., Tan I., Leung T., Lim L (1998) PAK kinases are directly coupled to the PIX family of nucleotide exchange factors. *Molecular Cell* **1**:183-192 https://doi.org/10.1016/s1097-2765(00)80019-2 | PubMed

Marcantoni A., Raymond E. F., Carbone E., Marie H (2014) Firing properties of entorhinal cortex neurons and early alterations in an Alzheimer's disease transgenic model. *Pflügers Archiv: European Journal of Physiology* **466**:1437-1450 https://doi.org/10.1007/s00424-013-1368-z | PubMed

Marilovtseva E. V., Abdurazakov A., Kurishev A. O., Mikhailova V. A., Golimbet V. E (2025) The role of GABA pathway components in pathogenesis of neurodevelopmental disorders. *International Journal of Molecular Sciences* **26**:9492 https://doi.org/10.3390/ijms26199492 | PubMed

Marín O (2012) Interneuron dysfunction in psychiatric disorders. *Nature Reviews Neuroscience* **13**:107-120 https://doi.org/10.1038/nrn3155 | PubMed

Marín O (2013) Cellular and molecular mechanisms controlling the migration of neocortical interneurons. *The European journal of neuroscience* **38**:2019-2029 https://doi.org/10.1111/ejn.12225 | PubMed

Marín O., Rubenstein J. L (2001) A long, remarkable journey: tangential migration in the telencephalon. *Nature reviews. Neuroscience* **2**:780-790 https://doi.org/10.1038/35097509 | PubMed

Martino A., Ettorre M., Musilli M., Lorenzetto E., Buffelli M., Diana G (2013) Rho GTPase-dependent plasticity of dendritic spines in the adult brain. *Frontiers in Cellular Neuroscience* **7**:62 https://doi.org/10.3389/fncel.2013.00062 | PubMed

Meseke M., Rosenberger G., Förster E (2013) Reelin and the Cdc42/Rac1 guanine nucleotide exchange factor αPIX/Arhgef6 promote dendritic Golgi translocation in hippocampal neurons. *The European Journal of Neuroscience* **37**:1404-1412 https://doi.org/10.1111/ejn.12153 | PubMed

Meyer M. A (2014) Highly expressed genes within hippocampal sector CA1: Implications for the physiology of memory. *Neurology International* **6**:5388 https://doi.org/10.4081/ni.2014.5388 | PubMed

Nishikawa M., Hayashi S., Nakayama A., Nishio Y., Shiraki A., Ito H., Maruyama K., Muramatsu Y., Ogi T., Mizuno S., *et al.* (2025) Pathophysiological significance of the p.E31G variant in RAC1 responsible for a neurodevelopmental disorder with microcephaly. *Biochimica et Biophysica Acta: Molecular Basis of Disease* **1871**:167520 https://doi.org/10.1016/j.bbadis.2024.167520 | PubMed

Nodé-Langlois R., Muller D., Boda B (2006) Sequential implication of the mental retardation proteins ARHGEF6 and PAK3 in spine morphogenesis. *Journal of Cell Science* **119**:4986-4993 https://doi.org/10.1242/jcs.03273 | PubMed

Paganoni A. J. J., Amoruso F., Porta Pelayo J., Calleja-Pérez B., Vezzoli V., Duminuco P., Caramello A., Oleari R., Fernández-Jaén A., Cariboni A (2022) A novel loss-of-function SEMA3E mutation in a patient with severe intellectual disability and cognitive regression. *International Journal of Molecular Sciences* **23**:5632 https://doi.org/10.3390/ijms23105632 | PubMed

Paredes M. F., James D., Gil-Perotin S., Kim H., Cotter J. A., Ng C., Sandoval K., Rowitch D. H., Xu D., McQuillen P. S., *et al.* (2016) Extensive migration of young neurons into the infant human frontal lobe. *Science* **354**:aaf7073 https://doi.org/10.1126/science.aaf7073 | PubMed

Paulsen B., Velasco S., Kedaigle A. J., Pigoni M., Quadrato G., Deo A. J., Adiconis X., Uzquiano A., Sartore R., Yang S. M., *et al.* (2022) Autism genes converge on asynchronous development of shared neuron classes. *Nature* **602**:268-273 https://doi.org/10.1038/s41586-021-04358-6 | PubMed

Pelkey K. A., Chittajallu R., Craig M. T., Tricoire L., Wester J. C., McBain C. J (2017) Hippocampal GABAergic inhibitory interneurons. *Physiological Reviews* **97**:1619-1747 https://doi.org/10.1152/physrev.00007.2017 | PubMed

Piton A., Redin C., Mandel J. L (2013) XLID-causing mutations and associated genes challenged in light of data from large-scale human exome sequencing. *American Journal of Human Genetics* **93**:368-383 https://doi.org/10.1016/j.ajhg.2013.06.013 | PubMed

Prakash N., Abu Irqeba A., Corbin J. G (2025) Development and function of the medial amygdala. *Trends in Neurosciences* **48**:22-32 https://doi.org/10.1016/j.tins.2024.11.004 | PubMed

Priolo M., Zara E., Radio F. C., Ciolfi A., Spadaro F., Bellacchio E., Mancini C., Pantaleoni F., Cordeddu V., Chiriatti L., *et al.* (2023) Clinical profiling of MRD48 and functional characterization of two novel pathogenic RAC1 variants. *European Journal of Human Genetics* **31**:805-814 https://doi.org/10.1038/s41431-023-01351-7 | PubMed

Ramakers G. J., Wolfer D., Rosenberger G., Kuchenbecker K., Kreienkamp H. J., Prange-Kiel J., Rune G., Richter K., Langnaese K., Masneuf S., *et al.* (2012) Dysregulation of Rho GTPases in the αPix/Arhgef6 mouse model of X-linked intellectual disability is paralleled by impaired structural and synaptic plasticity and cognitive deficits. *Human Molecular Genetics* **21**:268-286 https://doi.org/10.1093/hmg/ddr457 | PubMed

Reijnders M. R. F., Ansor N. M., Kousi M., Yue W. W., Tan P. L., Clarkson K., Clayton-Smith J., Corning K., Jones J. R., Lam W. W. K., *et al.* (2017) RAC1 missense mutations in developmental disorders with diverse phenotypes. *American Journal of Human Genetics* **101**:466-477 https://doi.org/10.1016/j.ajhg.2017.08.007 | PubMed

Sakai K., Miyazaki J.-i (1997) A transgenic mouse line that retains Cre recombinase activity in mature oocytes irrespective of the cre transgene transmission. *Biochemical and Biophysical Research Communications* **237**:318-324 https://doi.org/10.1006/bbrc.1997.7111 | PubMed

Sholl D. A (1953) Dendritic organization in the neurons of the visual and motor cortices of the cat. *Journal of Anatomy* **87**:387-406 PubMed

Sloan S. A., Andersen J., Paşca A. M., Birey F., Pașca S. P. (2018) Generation and assembly of human brain region-specific three-dimensional cultures. *Nature Protocols* **13**:2062-2085 https://doi.org/10.1038/s41596-018-0032-7 | PubMed

Southwell D. G., Paredes M. F., Galvao R. P., Jones D. L., Froemke R. C., Sebe J. Y., Alfaro-Cervello C., Tang Y., Garcia-Verdugo J. M., Rubenstein J. L., *et al.* (2012) Intrinsically determined cell death of developing cortical interneurons. *Nature* **491**:109-113 https://doi.org/10.1038/nature11523 | PubMed

Sun X., Wang L., Wei C., Sun M., Li Q., Meng H., Yue W., Zhang D., Li J (2021) Dysfunction of Trio GEF1 involves in excitatory/inhibitory imbalance and autism-like behaviors through regulation of interneuron migration. *Molecular Psychiatry* **26**:7621-7640 https://doi.org/10.1038/s41380-021-01109-x | PubMed

Tamamaki N., Yanagawa Y., Tomioka R., Miyazaki J., Obata K., Kaneko T (2003) Green fluorescent protein expression and colocalization with calretinin, parvalbumin, and somatostatin in the GAD67-GFP knock-in mouse. *The Journal of Comparative Neurology* **467**:60-79 https://doi.org/10.1002/cne.10905 | PubMed

Tejada-Simon M. V (2015) Modulation of actin dynamics by Rac1 to target cognitive function. *Journal of Neurochemistry* **133**:767-779 https://doi.org/10.1111/jnc.13100 | PubMed

Tivodar S., Kalemaki K., Kounoupa Z., Vidaki M., Theodorakis K., Denaxa M., Kessaris N., de Curtis I., Pachnis V., Karagogeos D. (2015) Rac-GTPases Regulate Microtubule Stability and Axon Growth of Cortical GABAergic Interneurons. *Cerebral cortex* **25**:2370-2382 https://doi.org/10.1093/cercor/bhu037 | PubMed

Uhlén M., Fagerberg L., Hallström B. M., Lindskog C., Oksvold P., Mardinoglu A., Sivertsson Å., Kampf C., Sjöstedt E., Asplund A., *et al.* (2015) Proteomics. Tissue-based map of the human proteome. *Science* **347**:1260419 https://doi.org/10.1126/science.1260419 | PubMed

Uhlen M., Zhang C., Lee S., Sjöstedt E., Fagerberg L., Bidkhori G., Benfeitas R., Arif M., Liu Z., Edfors F., *et al.* (2017) A pathology atlas of the human cancer transcriptome. *Science* **357**:eaan2507 https://doi.org/10.1126/science.aan2507 | PubMed

Umbach A., Maule G., Kheir E., Cutarelli A., Foglia M., Guarrera L., Fava L. L., Conti L., Garattini E., Terao M., *et al.* (2022) Generation of corrected hiPSC clones from a Cornelia de Lange syndrome (CdLS) patient through CRISPR-Cas-based technology. *Stem Cell Research & Therapy* **13**:440 https://doi.org/10.1186/s13287-022-03135-0 | PubMed

Upadia J., Liu J., Bier C., Chenevert M., Li Y (2025) Diverse clinical presentation of RAC1-related intellectual developmental disorder. *American Journal of Medical Genetics Part A* **197**:e63991 https://doi.org/10.1002/ajmg.a.63991 | PubMed

Vidaki M., Tivodar S., Doulgeraki K., Tybulewicz V., Kessaris N., Pachnis V., Karagogeos D (2012) Rac1-dependent cell cycle exit of MGE precursors and GABAergic interneuron migration to the cortex. *Cerebral Cortex* **22**:680-692 https://doi.org/10.1093/cercor/bhr145 | PubMed

Wang L., Wang C., Moriano J. A., Chen S., Zuo G., Cebrián-Silla A., Zhang S., Mukhtar T., Wang S., Song M., *et al.* (2025) Molecular and cellular dynamics of the developing human neocortex. *Nature* **647**:169-178 https://doi.org/10.1038/s41586-024-08351-7 | PubMed

Wonders C. P., Anderson S. A (2006) The origin and specification of cortical interneurons. *Nature reviews. Neuroscience* **7**:687-696 https://doi.org/10.1038/nrn1954 | PubMed

Wong F. K., Bercsenyi K., Sreenivasan V., Portalés A., Fernández-Otero M., Marín O (2018) Pyramidal cell regulation of interneuron survival sculpts cortical networks. *Nature* **557**:668-673 https://doi.org/10.1038/s41586-018-0139-6 | PubMed

Yang J., Yang X., Tang K (2022) Interneuron development and dysfunction. *The FEBS Journal* **289**:2318-2336 https://doi.org/10.1111/febs.15872 | PubMed

Yao Z., van Velthoven C. T. J., Nguyen T. N., Goldy J., Sedeno-Cortes A. E., Baftizadeh F., Bertagnolli D., Casper T., Chiang M., Crichton K., *et al.* (2021) A taxonomy of transcriptomic cell types across the isocortex and hippocampal formation. *Cell* **184**:3222-3241.e26 https://doi.org/10.1016/j.cell.2021.04.021 | PubMed

Yntema H. G., Hamel B. C., Smits A. P., van Roosmalen T., van den Helm B., Kremer H., Ropers H. H., Smeets D. F., van Bokhoven H. (1998) Localisation of a gene for non-specific X linked mental retardation (MRX46) to Xq25-q26. *Journal of Medical Genetics* **35**:801-805 https://doi.org/10.1136/jmg.35.10.801 | PubMed

Yoon S. J., Elahi L. S., Pașca A. M., Marton R. M., Gordon A., Revah O., Miura Y., Walczak E. M., Holdgate G. M., Fan H. C., *et al.* (2019) Reliability of human cortical organoid generation. *Nature Methods* **16**:75-78 https://doi.org/10.1038/s41592-018-0255-0 | PubMed

Zhou W., Li X., Premont R. T (2016) Expanding functions of GIT Arf GTPase-activating proteins, PIX Rho guanine nucleotide exchange factors and GIT-PIX complexes. *Journal of Cell Science* **129**:1963-1974 https://doi.org/10.1242/jcs.179465 | PubMed

Zuo Y., Oh W., Frost J. A (2014) Controlling the switches: Rho GTPase regulation during animal cell mitosis. *Cellular Signalling* **26**:2998-3006 https://doi.org/10.1016/j.cellsig.2014.09.022 | PubMed

Wang L, Wang C, Moriano J, Chen S, Zuo G, Cebrián-Silla A, Zhang S, Mukhtar T, Wang S, Song M, *et al.* (2025) Data from: Molecular and cellular dynamics of the developing human neocortex. Dryad Digital Repository. https://doi.org/10.5061/dryad.2280gb612

Yao Z, van Velthoven CTJ, Nguyen TN, Goldy J, Sedeno-Cortes AE, Baftizadeh F, Bertagnolli D, Casper T, Chiang M, Crichton K, *et al.* (2021) A taxonomy of transcriptomic cell types across the isocortex and hippocampal formation. Allen Institute for Brain Science. ID mouse-whole-cortex-and-hippocampus-smart-seq https://brain-map.org/our-research/cell-types-taxonomies/cell-types-database-rna-seq-data/mouse-whole-cortex-and-hippocampus-smart-seq

Peer reviews

Reviewer #1 (Public review):

Summary:

The manuscript has several strengths, including a technically comprehensive approach that combines mouse genetics, electrophysiology, live imaging in assembloids, and human organoid models, providing a rich and multifaceted dataset. Cross-species validation through the parallel use of mouse and human systems strengthens the generality of the observed phenotypes and increases relevance to human neurodevelopment.

Consistent phenotypic observations across systems show that ARHGEF6 loss affects migration, neurite morphology, growth cone structure, and neuronal survival, supporting a coherent role in cytoskeletal regulation.

There is clear evidence for developmental defects, including reduced interneuron numbers, increased apoptosis in the ganglionic eminences, and migration deficits, all well supported by quantitative analyses. Also, there is a high-quality electrophysiological characterization that demonstrates reduced firing in interneurons, providing a well-controlled functional phenotype.

Strengths:

The manuscript has several strengths, including a technically comprehensive approach that combines mouse genetics, electrophysiology, live imaging in assembloids, and human organoid models, providing a rich and multifaceted dataset. Cross-species validation through the parallel use of mouse and human systems strengthens the generality of the observed phenotypes and increases relevance to human neurodevelopment.

Consistent phenotypic observations across systems show that ARHGEF6 loss affects migration, neurite morphology, growth cone structure, and neuronal survival, supporting a coherent role in cytoskeletal regulation.

There is clear evidence for developmental defects, including reduced interneuron numbers, increased apoptosis in the ganglionic eminences, and migration deficits, all well supported by quantitative analyses. Also, there is a high-quality electrophysiological characterization that demonstrates reduced firing in interneurons, providing a well-controlled functional phenotype.

Weaknesses:

Despite the strengths mentioned above, the study has some conceptual and experimental weaknesses that reduce its impact. The mechanistic insight is limited, as the research does not directly establish how ARHGEF6 regulates downstream signaling pathways.

Also, there is insufficient evidence for interneuron specificity; although the central claim is that ARHGEF6 plays a selective role in interneurons, the data do not adequately exclude the possibility that the observed effects reflect broader neuronal defects. The study lacks critical controls across cell types, as several phenotypes observed in organoids and progenitors, including apoptosis, reduced neuronal output, and altered morphology, could also affect multiple neuronal populations without being directly tested. Furthermore, the data are predominantly descriptive, with many results remaining correlative and failing to establish causal relationships.

Some more comments:

(1) Given that ARHGEF6 is a guanine nucleotide exchange factor for Rac1 and Cdc42, the absence of direct measurements of GTPase activity or downstream signaling represents a significant gap. The interpretation that the observed phenotypes are mediated through specific cytoskeletal pathways, therefore, remains inferential.

(2) The manuscript repeatedly interprets the findings as interneuron-specific. However, several key observations are not demonstrated to be restricted to IN. Without direct comparison to excitatory neurons or other cell types, it is difficult to conclude that ARHGEF6 plays a selective role in interneurons rather than a more general role in neuronal development. The well-done analysis of the transcriptomic dataset is not sufficient to claim IN specificity. This issue is particularly important for the interpretation of the human organoid experiments, where reductions in $SOX2^{+}$ progenitors and $NEUN^{+}$ neurons, as well as increased apoptosis, could reflect global developmental defects. Similarly, in the mouse experiments, the reduction in $GAD67^{+}$ cells is compelling, but it is not shown whether other neuronal populations are also affected.

(3) The study provides a strong phenotypic description but limited causal resolution. For example, migration defects, altered growth cone morphology, and reduced branching are all consistent with impaired cytoskeletal regulation, but the links between these phenotypes are not directly established. Likewise, while the electrophysiological data convincingly show reduced firing in interneurons, the connection between altered cytoskeletal dynamics and intrinsic excitability is not explored.

(4) Several aspects of data presentation could be improved. In multiple figures (e.g., Figure 1A, D; Figure 4 and Video S1, 2), the images are difficult to interpret due to high cellular density, limited magnification, or lack of clear annotation. In some cases, it is not fully clear how quantifications were performed or which regions were analyzed. Improving the visual clarity with arrows, boxes, and high-magnification inserts of the data would strengthen confidence in the conclusions.

https://doi.org/10.7554/eLife.111288.1.sa3

Reviewer #2 (Public review):

The authors investigate the impact of the deletion of the small GTPase regulator ARHGEF6 on the development and physiology of interneurons. Using public databases, they first show that ARHGEF6 is enriched in interneurons or in areas that give rise to them, both in development and adulthood, in humans and mice. Using a complete KO mouse previously reported, and using a GAD67-GFP reporter mice line, they show that in the adult mouse cortex and hippocampus, there is a notorious reduction GFP+ cells. These mice show increased apoptotic cells at different timepoints and areas of the brain during development. In the developing cortex of ARHGEF6-KO mice, there are fewer IN in all layers of the developing cortex, and cells present processes not correctly oriented. IN from the hippocampus in culture show reduced excitability and impaired neurite branching. The authors then established isogenic hiPSCs lines to study ARHGEF6 deletion in human cells and differentiated ventral forebrain neurons, to find interneuron-related and non-related phenotypes. Most importantly, human interneurons grown in organoids show reduced branching and altered growth cone morphology. The authors claim that the novel interneuron phenotypes found in these models can explain, in part, the human intellectual disabilities associated with mutations in this protein. The study is well conducted and opens new avenues of research not only for the role of small GTPases regulation in early nervous system development, but also for how interneuron deficiencies impact a wider range of intellectual disability syndromes found in humans.

However, most conclusions of the present version would be strengthened after considering the following comments:

Major comments

(1) The reported biological processes evaluated at different developmental stages may be directly or indirectly related to ARHGEF6 function itself. As a model of a hereditary disease, full organism gene deletion is valid, since the human patients suffer from that condition as well. However, to investigate the roles of a protein, complete deletions may not be very accurate since they can give rise to phenotypes that are only indirectly related to the protein function itself. Most conclusions of the present manuscript should either be discussed in this regard or add evidence for a direct role of the protein. One such evidence is typically performed with acute knockdowns in culture, or in developing brains by in utero electroporation. For example, Figure 1C shows that the principal excitatory neurons in the hippocampus do not express ARHGEF6. However, most electrophysiological and behavioral evidence of defects in ARHGEF6-KO mice arises from evaluating these cells (Remakers et al., 2012). I am not suggesting that either previous or actual evidence is wrong. But I believe readers would benefit from a clear distinction (or add caution notes) between a functional consequence of the deletion (that can be months away and in other cells than the actual molecular defect) and a true cell biological function of the protein under study. In favor of the authors, this is a concern with most conclusions derived from KO organisms.

(2) Figure 1E-G H I. All conclusions are made with a GAD67-GFP reporter, which is a very powerful and reliable tool for large-scale screening. All the conclusions of the paper would be

strengthened if some immunohistochemical staining in the same areas of specific markers for interneurons would be added as supporting complementary evidence.

(3) Cell death in development: It is surprising that the high amount of TUNEL staining during development does not translate into gross histological changes in the adult brain (studied elsewhere). Can authors discuss possible explanations?

(4) Section 4 (Figures 2F-J) - The authors present this staining as an analysis of migration. Normally, migration studies are performed with a "pulse-chase" paradigm, where a single cohort is labeled and then followed over time (normally by in utero electroporation of a fluorescent protein). Tissue is then fixed at different time points, and migration can be followed. On the contrary, the evidence is from a single point, in an experimental setting in which all Gad67 IN are stained, and hence, one cannot imply a defect in migration. The differences between WT and ARHGEF6-KO are obvious and interesting; it is just that they cannot be solely attributed to a problem in migration.

Also, a true phenotype of migration in the current setting should have found that the cells that failed to migrate are accumulated in deeper layers. My impression is that the changes in IN per layer are easier explained by total cell number, rather than migration. Perhaps evaluating earlier timepoints could clarify this.

(5) It is known that ARHGEF6 deletion produces severe F-actin phenotypes in neurons. Have the authors confirmed in their hippocampal cultures GAD67 cells ALSO have these phenotypes? Stress fibers in somas, growth cones, and actin patches along neurites.

(6) Section 4. The authors present data for deficient migration of the GFP-labeled interneurons. Is it possible to assess, in the same sections, whether other cell types are also affected? Although the hypothesis that ARHGEF6 deletion will have an impact in IN is well rooted in expression data, by assessing other cell types, one can even include a positive control or evidence for a cell-autonomous phenotype.

(7) ARHGEDF6 deletion has an important impact on organoid development (size, shape, etc). Have the authors analysed whether these organoids produced fewer interneurons?

(8) In assembloids, the differences in migration parameters are very small between WT and ARHGEF6-KO, which reinforces that perhaps what is observed in the different layers of cortex during mouse development is likely not entirely due to migration, as concluded.

(9) To properly weigh the present evidence -interneuron deficits- using the ARHGEF6-KO model, authors should include a deeper discussion in light of much work that has been done using these mice. How does the finding of a diminished IN population in the brain of these mice explain the large amount of electrophysiological and behavioral evidence produced before with these animals? Perhaps the most important work to discuss these aspects is the initial ARHGEF6-KO report by Ramakers and colleagues (2012), but there are others.

Minor comments

(1) Figure 1A. It looks clear that the GE shows the highest expression of ARHGEF6; however, the reader needs the reference levels where the log2 expression is calculated. What are the reference levels?

(2) Have the authors compared the number of GAD67-eGFP cells in the hippocampal cultures between WT and ARHGEF6-KO mice?

(3) Section 3, as a caution note, authors should mention that it is not possible to know from the evidence provided which cells are dying.

(4) In the dorsal-ventral assembloids, it is expected that the ventral organoid would contain lots of GFP expression compared to the dorsal, but in the image shown (Figure 5A) both parts of the assembloid seem to have the same amount and distribution of GFP. How is that possible?

https://doi.org/10.7554/eLife.111288.1.sa2

Reviewer #3 (Public review):

Summary:

ARHGEF6 is a RAC1/CDC42 guanine nucleotide exchange factor that has been proposed to be associated with X-linked intellectual disability, but its relevance to the pathology is not well established. ARHGEF6 has been assigned a role in spine density and plasticity of hippocampal pyramidal neurons, but nothing is known about its role in interneuron development. Here, the authors show that ARHGEF6 is expressed early in development in the inhibitory lineage during the peak of interneuron generation and migration. The aim of the study is therefore to investigate whether, in addition to its role in pyramidal neurons, ARHGEF6 could play a role in inhibitory neuron development. Using both ARHGEF6-KO mice and organoids from ARHGEF6-KO hiPSCs, the authors show that ARHGEF6 plays a critical role in interneuron development and function

Strengths:

The major strength of the paper is the very detailed analysis of the role of ARHGEF6 using two different systems: ARHGEF6-KO mice and deletion of ARHGEF6 in human iPSC-derived organoids. Strikingly, deletion of ARHGEF6 in both systems induces similar defects such as an increase in apoptosis, reduced neuronal output, impaired neuronal morphology, and disrupted migratory dynamics. This compelling evidence demonstrates that ARHGEF6, in addition to its already well-described role in spine formation and plasticity, is playing a crucial role during embryonic development through its function in interneurons.

Weaknesses:

(1) In Figure 1, the authors show that ARHGEF6 is expressed in different regions of the brain, including the interneuron lineage, and that depletion of ARHGEF6 reduces the number of GABAergic neurons in the adult cortex and hippocampus. To try to better characterize this defect, the authors in Figure 2 investigate whether deletion of ARHGEF6 affects interneuron migration and survival during embryonic development. To do so, ARHGEF6 ko mice were crossed with the GAD67-eGFP reporter line to follow the inhibitory lineage. The authors analyse apoptosis using TUNEL staining, and show that it is significantly increased in the ganglion eminence of ARHGEF6-KO E14.5 embryos. The authors claim that this is not the case in the cortex. However, the image shown in Figure 2A really suggests that staining is increased. Which part of the neocortex is analysed for quantification? This should be clarified.

(2) In Figure 2F-J, the authors investigate the migration of interneurons by analysing the GAD67-eGFP staining, and clearly show that the migratory abilities of the depleted neurons are reduced. However, the authors do not discuss the fact that, because depletion of ARHGEF6 increases apoptosis, there are fewer neurons available for migration. This is important for the interpretation of the data. This point should be clarified.

(3) In Supplementary Figure S2, the authors describe the establishment of the ARHGEF6-KO human iPSC line and test the ability of these cells to undergo correct development, especially for the generation of neural progenitor cells. I was wondering why the authors do not present the data of both control and ARHGEF6-KO cells.

(4) At the molecular level, how ARHGEF6 depletion could affect neuronal survival is missing. In addition, as ARHGEF6 is a GEF for RAC1 and Cdc42 amongst other GEFs, I would have expected that the authors test how RAC1 activity (and Cdc42) is affected in ARHGEF6-depleted brains and in ARHGEF6-KO organoids. The measure of phalloidin staining and the anisotropy index are not really meaningful.

(5) The authors show that ARHGEF6-KO forebrain organoids were markedly smaller compared to their isogenic controls, and their study suggests that ARHGEF6 expression impacts progenitor maintenance and neurogenesis. Despite representing only a minority of the total neuronal population, I was wondering whether ARHGEF6-KO mice present brain morphology defects such as microcephaly.

https://doi.org/10.7554/eLife.111288.1.sa1

Author response:

Public Reviews:

Reviewer #1 (Public review):

Summary:

The manuscript has several strengths, including a technically comprehensive approach that combines mouse genetics, electrophysiology, live imaging in assembloids, and human organoid models, providing a rich and multifaceted dataset. Cross-species validation through the parallel use of mouse and human systems strengthens the generality of the observed phenotypes and increases relevance to human neurodevelopment.

Consistent phenotypic observations across systems show that ARHGEF6 loss affects migration, neurite morphology, growth cone structure, and neuronal survival, supporting a coherent role in cytoskeletal regulation.

There is clear evidence for developmental defects, including reduced interneuron numbers, increased apoptosis in the ganglionic eminences, and migration deficits, all well supported by quantitative analyses. Also, there is a high-quality electrophysiological characterization that demonstrates reduced firing in interneurons, providing a well-controlled functional phenotype.

Strengths:

The manuscript has several strengths, including a technically comprehensive approach that combines mouse genetics, electrophysiology, live imaging in assembloids, and human organoid models, providing a rich and multifaceted dataset. Cross-species validation through the parallel use of mouse and human systems strengthens the generality of the observed phenotypes and increases relevance to human neurodevelopment.

Consistent phenotypic observations across systems show that ARHGEF6 loss affects migration, neurite morphology, growth cone structure, and neuronal survival, supporting a coherent role in cytoskeletal regulation.

There is clear evidence for developmental defects, including reduced interneuron numbers, increased apoptosis in the ganglionic eminences, and migration deficits, all well supported by quantitative analyses. Also, there is a high-quality electrophysiological characterization that demonstrates reduced firing in interneurons, providing a well-controlled functional phenotype.

We thank the reviewer for their positive and thoughtful assessment of our manuscript. We appreciate their recognition of the technical breadth of the study, including the integration of mouse genetics, electrophysiology, live imaging in assembloids, and human organoid models. We are also grateful that the reviewer highlights the value of our cross-species approach, as a major goal of the study was to determine whether ARHGEF6 loss produces convergent developmental and cellular phenotypes in both mouse and human systems.

> *Weaknesses:*
>
> *Despite the strengths mentioned above, the study has some conceptual and experimental weaknesses that reduce its impact. The mechanistic insight is limited, as the research does not directly establish how ARHGEF6 regulates downstream signaling pathways.*

We appreciate the reviewer's constructive comment. We agree that, although our data establish a phenotypic link between ARHGEF6 loss and interneuron development, they do not directly dissect the molecular mechanisms underlying the observed defects. Our interpretation that the mutant phenotype involves dysregulation of cytoskeletal dynamics is based on the directly observed defects in actin polymerization and organization in neural progenitor cells and neuronal growth cones respectively, and is consistent with the abnormalities observed in neurite morphology and neuronal migration. This interpretation is further supported by the established role of Arhgef6 as a regulator of the small Rho GTPases Rac1 and Cdc42. Previous evidence shows that Arhgef6 loss reduces the activity of both GTPases and deregulates the expression of the cytoskeletal regulators Pak1–3, Limk1, and Cofilin in the mouse brain (Ramakers et al., 2012). Moreover, spine abnormalities in *Arhgef6*-knockdown *ex vivo* slice cultures can be rescued by expressing the active form of Pak3, a downstream effector of Rac1 and Cdc42 (Node-Langlois et al., 2006). Together, these findings support a model in which the loss of the protein affects development through cytoskeletal dysregulation, likely involving altered Rho GTPase signalling. We nevertheless agree that further experiments would be required to establish a direct causal relationship between ARHGEF6 loss, Rho GTPase activity, cytoskeletal dysregulation, and the interneuron phenotypes described here. We will therefore revise the manuscript to clarify that this mechanistic link remains an interpretation supported by our data and the literature, rather than a direct demonstration within the present study.

> *Also, there is insufficient evidence for interneuron specificity; although the central claim is that ARHGEF6 plays a selective role in interneurons, the data do not adequately exclude the possibility that the observed effects reflect broader neuronal defects. The study lacks critical controls across cell types, as several phenotypes observed in organoids and progenitors, including apoptosis, reduced neuronal output, and altered morphology, could also affect multiple neuronal populations without being directly tested.*

We agree that the current data do not exclude the possibility of alterations in other neuronal lineages, specifically the excitatory lineage. With regard to this, we would like to emphasize that the investigation of excitatory cell phenotypes was beyond the scope of the present study, as this aspect has previously been examined by Ramakers et al., 2012 and Node-Langlois et al., 2006, particularly in the context of hippocampal pyramidal cells, which are among the few cell types showing consistent expression of the gene in the adult mouse brain (Allen Brain Atlas; Yao et al., 2021). In this context, it is interesting to note that, in Ramakers et al., 2012 (Figure S1), MAP2 immunostaining of hippocampal formations revealed comparable distribution and intensity of neuronal cell bodies and dendrites throughout the hippocampus of both wild-type and *Arhgef6*-KO animals. With regard to morphological maturation of excitatory cells, whereas we observe a simplification of interneuron morphology in both mouse and human models, Ramakers et al., 2012 reported increased dendritic arborization complexity in hippocampal pyramidal cells. With regard to migration, a direct comparison

with excitatory neurons would be intrinsically difficult, as excitatory and inhibitory neurons undergo highly distinct migratory processes and are therefore not directly comparable. We greatly appreciate the reviewer's comment, as it gives us the opportunity to better discuss the relationship between our findings and previous studies in the Discussion. We will revise the manuscript and avoid implying that the phenotype observed is exclusive to interneurons.

> *Furthermore, the data are predominantly descriptive, with many results remaining correlative and failing to establish causal relationships.*

We agree that our study primarily establishes a phenotypic framework and does not fully resolve the causal hierarchy among altered survival, migration, cytoskeletal morphology, and intrinsic excitability. We will revise the manuscript to make this limitation explicit, avoiding statements that imply direct causality beyond the data presented.

> *Some more comments:*
>
> *(1) Given that ARHGEF6 is a guanine nucleotide exchange factor for Rac1 and Cdc42, the absence of direct measurements of GTPase activity or downstream signaling represents a significant gap. The interpretation that the observed phenotypes are mediated through specific cytoskeletal pathways, therefore, remains inferential.*

We appreciate the comment. The interpretation that our phenotype involves dysregulated cytoskeletal dynamics is based on the observed defects in actin polymerization and F-actin organization in neuronal growth cones and is consistent with the abnormalities in neurite morphology and neuronal migration. We will explicitly state in the Discussion that, since we did not directly measure Rac1 and Cdc42 activity levels in our models, our hypothesis regarding the involvement of this molecular pathway in the establishment of the observed phenotype therefore remains inferential, despite being supported by the current literature.

> *(2) The manuscript repeatedly interprets the findings as interneuron-specific. However, several key observations are not demonstrated to be restricted to IN. Without direct comparison to excitatory neurons or other cell types, it is difficult to conclude that ARHGEF6 plays a selective role in interneurons rather than a more general role in neuronal development. The well-done analysis of the transcriptomic dataset is not sufficient to claim IN specificity. This issue is particularly important for the interpretation of the human organoid experiments, where reductions in SOX2$^+$ progenitors and NEUN$^+$ neurons, as well as increased apoptosis, could reflect global developmental defects. Similarly, in the mouse experiments, the reduction in GAD67$^+$ cells is compelling, but it is not shown whether other neuronal populations are also affected.*

As previously mentioned, we understand the reviewer's concern regarding the specificity of the observed phenotypes in interneurons and agree that the claims should be tempered. However, it is important to note that the interpretation of the human organoid experiments should be reconsidered. The use of specifically ventralized MGE-like organoids allowed us to assess the cell-autonomous nature of defects such as the reduction in inhibitory progenitors' neuronal output, the increased apoptosis, and the morphological abnormalities of inhibitory neurons. We will acknowledge in the Discussion the limitations of the study with regard to assessing the cell-autonomous nature of the observed migration defects.

> *(3) The study provides a strong phenotypic description but limited causal resolution. For example, migration defects, altered growth cone morphology, and reduced branching are all consistent with impaired cytoskeletal regulation, but the links between these phenotypes are not directly established. Likewise, while the electrophysiological data convincingly show reduced firing in interneurons, the connection between altered cytoskeletal dynamics and intrinsic excitability is not explored.*

The observed migration defects, altered growth-cone morphology, and reduced branching are consistent with impaired cytoskeletal regulation. However, we acknowledge that the mechanistic links among these phenotypes remain to be directly demonstrated. Similarly, although our electrophysiological data show reduced firing in *ARHGEF6*-KO interneurons, the present study does not provide direct evidence linking impaired excitability to altered cytoskeletal dynamics. In the latter case, we think that the underlying mechanisms should be further investigated at the subcellular level, particularly with respect to cytoskeleton-mediated intracellular trafficking and localization and distribution of ion channels. One limitation of the present study, which may have masked electrophysiological alterations associated with differences in membrane composition (current Figure S1D–H), is that different interneuron subtypes with distinct intrinsic properties were pooled together in the analysis. We will expand the Discussion to address these limitations.

> *(4) Several aspects of data presentation could be improved. In multiple figures (e.g., Figure 1A, D; Figure 4 and Video S1, 2), the images are difficult to interpret due to high cellular density, limited magnification, or lack of clear annotation. In some cases, it is not fully clear how quantifications were performed or which regions were analyzed. Improving the visual clarity with arrows, boxes, and high-magnification inserts of the data would strengthen confidence in the conclusions.*

We would like to thank the reviewer for pointing this out. We agree that some images and videos would benefit from clearer annotation. In the revised manuscript, we will add high-magnification insets, arrows or boxes highlighting the relevant regions/cells, and clearer descriptions of the quantified regions. We will also improve legends and video labels to indicate genotype, region, and tracked cells.

> ***Reviewer #2 (Public review):***
>
> *The authors investigate the impact of the deletion of the small GTPase regulator ARHGEF6 on the development and physiology of interneurons. Using public databases, they first show that ARHGEF6 is enriched in interneurons or in areas that give rise to them, both in development and adulthood, in humans and mice. Using a complete KO mouse previously reported, and using a GAD67-GFP reporter mice line, they show that in the adult mouse cortex and hippocampus, there is a notorious reduction GFP+ cells. These mice show increased apoptotic cells at different timepoints and areas of the brain during development. In the developing cortex of ARHGEF6-KO mice, there are fewer IN in all layers of the developing cortex, and cells present processes not correctly oriented. IN from the hippocampus in culture show reduced excitability and impaired neurite branching. The authors then established isogenic hiPSCs lines to study ARHGEF6 deletion in human cells and differentiated ventral forebrain neurons, to find interneuron-related and non-related phenotypes. Most importantly, human interneurons grown in organoids show reduced branching and altered growth cone morphology. The authors claim that the novel interneuron phenotypes found in these models can explain, in part, the human intellectual disabilities associated with mutations in this protein. The study is well conducted and opens new avenues of research not only for the role of small GTPases regulation in early nervous system development, but also for how interneuron deficiencies impact a wider range of intellectual disability syndromes found in humans.*

We appreciate the reviewer's positive evaluation of our manuscript and their recognition of this work's potential to expand the focus of intellectual disability research on the development and function of the inhibitory system. We are particularly encouraged that the reviewer highlights the strength of our combined mouse and human cellular models, as well as the relevance of the interneuron-related phenotypes we identify across systems.

> *However, most conclusions of the present version would be strengthened after considering the following comments:*
>
> *Major comments:*
>
> *(1) The reported biological processes evaluated at different developmental stages may be directly or indirectly related to ARHGEF6 function itself. As a model of a hereditary disease, full organism gene deletion is valid, since the human patients suffer from that condition as well. However, to investigate the roles of a protein, complete deletions may not be very accurate since they can give rise to phenotypes that are only indirectly related to the protein function itself. Most conclusions of the present manuscript should either be discussed in this regard or add evidence for a direct role of the protein. One such evidence is typically performed with acute knockdowns in culture, or in developing brains by in utero electroporation. For example, Figure 1C shows that the principal excitatory neurons in the hippocampus do not express ARHGEF6. However, most electrophysiological and behavioral evidence of defects in ARHGEF6-KO mice arises from evaluating these cells (Ramakers et al., 2012). I am not suggesting that either previous or actual evidence is wrong. But I believe readers would benefit from a clear distinction (or add caution notes) between a functional consequence of the deletion (that can be months away and in other cells than the actual molecular defect) and a true cell biological function of the protein under study. In favor of the authors, this is a concern with most conclusions derived from KO organisms.*

We agree with the reviewer that phenotypes observed in constitutive knockout models may, in some contexts, reflect indirect or compensatory consequences of long-term gene loss. Conditional and/or inducible knockout or knockdown approaches can certainly help dissect the nature of the observed defects and better define the effects of gene ablation at different developmental stages or in specific cell types. However, in the context of our study, it is important to note that the experiments performed in ventralized MGE-like organoids allowed us to assess the cell-autonomous nature of very early developmental defects in the inhibitory lineage, in isolation from other cell types. These defects include reduced neuronal output from inhibitory progenitors, increased apoptosis, and morphological abnormalities in inhibitory neurons. Therefore, the phenotypes reported here are less likely to reflect effects originating in, or indirectly caused by, cell types that do not express *Arhgef6*.

With regard to Figure 1C, we state in the Results that “among excitatory populations, only CA3 pyramidal neurons and mossy cells exhibited expression levels comparable to those observed in inhibitory clusters (Figure 1D, Table S2),” thereby not neglecting the potential effect of the lack of a functional protein in these populations.

> *(2) Figure 1E-G H I. All conclusions are made with a GAD67-GFP reporter, which is a very powerful and reliable tool for large-scale screening. All the conclusions of the paper would be strengthened if some immunohistochemical staining in the same areas of specific markers for interneurons would be added as supporting complementary evidence.*

We appreciate the insightful comment of the reviewer. Additional validation using established interneuronal markers will further strengthen the GAD67-eGFP analysis. We will perform complementary stainings (e.g., PVALB and CCK) and quantifications and include these data as a Supplementary Figure.

> *(3) Cell death in development: It is surprising that the high amount of TUNEL staining during development does not translate into gross histological changes in the adult brain (studied elsewhere). Can authors discuss possible explanations?*

We appreciate the thoughtful consideration of our findings. We think that possible explanations include partial compensatory mechanisms during development, which may mitigate the long-term anatomical consequences of increased cell death. In addition, the phenotype may be restricted to specific neuronal populations or developmental windows, thereby producing functional alterations without necessarily resulting in overt macroanatomical defects. Thus, although increased developmental cell death may contribute to altered circuit assembly and neuronal output, it may not be sufficient to produce gross histological changes detectable at the adult brain level.

> *(4) Section 4 (Figures 2F-J) - The authors present this staining as an analysis of migration. Normally, migration studies are performed with a "pulse-chase" paradigm, where a single cohort is labeled and then followed over time (normally by in utero electroporation of a fluorescent protein). Tissue is then fixed at different time points, and migration can be followed. On the contrary, the evidence is from a single point, in an experimental setting in which all Gad67 IN are stained, and hence, one cannot imply a defect in migration. The differences between WT and ARHGEF6-KO are obvious and interesting; it is just that they cannot be solely attributed to a problem in migration.*
>
> *Also, a true phenotype of migration in the current setting should have found that the cells that failed to migrate are accumulated in deeper layers. My impression is that the changes in IN per layer are easier explained by total cell number, rather than migration. Perhaps evaluating earlier timepoints could clarify this.*

We appreciate the reviewer's suggestion to implement an additional time point in the *in vivo* migration analysis. Since an earlier *in vivo* time point would most likely not reveal migration-related defects, as most cells would still be confined to the ganglionic eminence (Liaci et al., 2022), we will include analyses performed at a later developmental time point as supplementary evidence. We will also revise the wording to clarify that the fixed-tissue data show altered distribution and orientation of GAD67-eGFP-positive interneurons, which are consistent with impaired migratory behavior when considered together with the *in vitro* live-imaging data. At the same time, we will acknowledge that reduced interneuron survival and/or neuronal output may also contribute to the observed phenotype.

> *(5) It is known that ARHGEF6 deletion produces severe F-actin phenotypes in neurons. Have the authors confirmed in their hippocampal cultures GAD67 cells ALSO have these phenotypes? Stress fibers in somas, growth cones, and actin patches along neurites.*

We did not directly assess F-actin organization in GAD67-eGFP murine primary cultures. Direct analyses of F-actin organization, growth-cone morphology, and cytoskeletal organization were performed only in the human system. To further assess this phenotype, we will perform phalloidin staining on GAD67-eGFP brain sections to evaluate F-actin organization in interneurons *in vivo*.

> *(6) Section 4. The authors present data for deficient migration of the GFP-labeled interneurons. Is it possible to assess, in the same sections, whether other cell types are also affected? Although the hypothesis that ARHGEF6 deletion will have an impact in IN is well rooted in expression data, by assessing other cell types, one can even include a positive control or evidence for a cell-autonomous phenotype.*

We thank the reviewer for their thoughtful suggestions. We agree that extending the analysis to additional cell types would provide further insight into the specificity of the phenotype; however, a comprehensive evaluation of all neuronal populations falls beyond the scope of this research. The use of ventralized MGE-like organoids enabled us to examine whether key defects were cell-autonomous, including the reduced neuronal output of inhibitory progenitors, increased apoptosis, and abnormal inhibitory-neuron morphology.

> *(7) ARHGEDF6 deletion has an important impact on organoid development (size, shape, etc). Have the authors analysed whether these organoids produced fewer interneurons?*

We would like to clarify that the organoids analyzed in the study are ventral MGE-like organoids and therefore the reduction in neuronal output (current Figure 4K) primarily reflects the ventral/interneuron lineage in this model.

> *(8) In assembloids, the differences in migration parameters are very small between WT and ARHGEF6-KO, which reinforces that perhaps what is observed in the different layers of cortex during mouse development is likely not entirely due to migration, as concluded.*

We agree that the migration parameters in assembloids should not be interpreted in isolation. We will revise the text to emphasize that the reduction in the number of interneurons observed in the adult brains is part of a broader pattern that also includes altered neuronal output and reduced viability.

> *(9) To properly weigh the present evidence -interneuron deficits- using the ARHGEF6-KO model, authors should include a deeper discussion in light of much work that has been done using these mice. How does the finding of a diminished IN population in the brain of these mice explain the large amount of electrophysiological and behavioral evidence produced before with these animals? Perhaps the most important work to discuss these aspects is the initial ARHGEF6-KO report by Ramakers and colleagues (2012), but there are others.*

We appreciate the reviewer's emphasis on the importance of framing our findings within the broader context of the existing literature. We will expand the Discussion to better integrate previous work on *ARHGEF6*-KO mice. Specifically, we will discuss how reduced interneuron number and altered interneuronal function may contribute to previously reported electrophysiological and behavioral phenotypes, acting in concert with previously described alterations in excitatory neurons and synaptic plasticity (Ramakers et al., 2012).

> *Minor comments:*
>
> *(1) Figure 1A. It looks clear that the GE shows the highest expression of ARHGEF6; however, the reader needs the reference levels where the log2 expression is calculated. What are the reference levels?*

We would like to thank the reviewer for pointing this out. We will clarify in the caption that the log2(RPKM+1) expression values are shown as absolute values and are not relative to a reference condition.

> *(2) Have the authors compared the number of GAD67-eGFP cells in the hippocampal cultures between WT and ARHGEF6-KO mice?*

We did not rely on total GAD67-eGFP counts in dissociated hippocampal cultures because differences could reflect initial plating composition, survival, and maturation. In our experience, the MGE-like organoid system provides a more controlled *in vitro* context to assess neuronal output in the ventral lineage.

> *(3) Section 3, as a caution note, authors should mention that it is not possible to know from the evidence provided which cells are dying.*

We agree with the reviewer and will add a cautionary statement noting that TUNEL staining alone does not identify the precise dying cell type. We will clarify that increased cell death in the ganglionic eminence and MGE-like organoids is consistent with a prominent involvement of the ventral/inhibitory lineage, while acknowledging the limits of the assay.

> *(4) In the dorsal-ventral assembloids, it is expected that the ventral organoid would contain lots of GFP expression compared to the dorsal, but in the image shown (Figure 5A) both parts of the assembloid seem to have the same amount and distribution of GFP. How is that possible?*

We appreciate the thoughtful comment of the reviewer. After two weeks of fusion, a considerable number of interneurons are expected to have migrated from the ventral to the dorsal compartment of the assembloid (Birey et al., 2017; Sloan et al., 2018). In terms of distribution, we think that current Figure 5A shows a gradient of eGFP-positive cells within the dorsal compartment, with the number of labeled cells decreasing as the distance from the fusion interface between the two organoids increases. By contrast, a comparable gradient is not evident in the ventral compartment, where several labeled neurons remain present even in regions distal to the fusion site.

> ***Reviewer #3 (Public review):***
>
> *Summary:*
>
> *ARHGEF6 is a RAC1/CDC42 guanine nucleotide exchange factor that has been proposed to be associated with X-linked intellectual disability, but its relevance to the pathology is not well established. ARHGEF6 has been assigned a role in spine density and plasticity of hippocampal pyramidal neurons, but nothing is known about its role in interneuron development. Here, the authors show that ARHGEF6 is expressed early in development in the inhibitory lineage during the peak of interneuron generation and migration. The aim of the study is therefore to investigate whether, in addition to its role in pyramidal neurons, ARHGEF6 could play a role in inhibitory neuron development. Using both ARHGEF6-KO mice and organoids from ARHGEF6-KO hiPSCs, the authors show that ARHGEF6 plays a critical role in interneuron development and function*
>
> *Strengths:*
>
> *The major strength of the paper is the very detailed analysis of the role of ARHGEF6 using two different systems: ARHGEF6-KO mice and deletion of ARHGEF6 in human iPSC-derived organoids. Strikingly, deletion of ARHGEF6 in both systems induces similar defects such as an increase in apoptosis, reduced neuronal output, impaired neuronal morphology, and disrupted migratory dynamics. This compelling evidence demonstrates that ARHGEF6, in addition to its already well-described role in spine formation and plasticity, is playing a crucial role during embryonic development through its function in interneurons.*

We thank the reviewer for this positive assessment of our work and for highlighting the strength of our combined *in vivo* and human iPSC-derived organoid approaches. We are pleased that the reviewer recognizes the consistency of the phenotypes observed across both systems and acknowledges that our findings support a crucial role, during early stages of embryonic development, for a protein previously thought to be relevant primarily in the synaptic context.

> *Weaknesses:*
>
> *(1) In Figure 1, the authors show that ARHGEF6 is expressed in different regions of the brain, including the interneuron lineage, and that depletion of ARHGEF6 reduces the number of GABAergic neurons in the adult cortex and hippocampus. To try to better characterize this defect, the authors in Figure 2 investigate whether deletion of ARHGEF6 affects interneuron migration and survival during embryonic development. To do so, ARHGEF6 ko mice were crossed with the GAD67-eGFP reporter line to follow the inhibitory lineage. The authors analyse apoptosis using TUNEL staining, and show that it is*

> *significantly increased in the ganglion eminence of ARHGEF6-KO E14.5 embryos. The authors claim that this is not the case in the cortex. However, the image shown in Figure 2A really suggests that staining is increased. Which part of the neocortex is analysed for quantification? This should be clarified.*

We would like to thank the reviewer for pointing this out. The region analyzed was the same as that used to assess GAD67-eGFP-positive cells in Figure 2F. We will clarify the exact neocortical region used for TUNEL quantification and revise the figure and legend to make the analyzed area explicit. We will also analyze additional animals to improve the accuracy of the analysis.

> *(2) In Figure 2F-J, the authors investigate the migration of interneurons by analysing the GAD67-eGFP staining, and clearly show that the migratory abilities of the depleted neurons are reduced. However, the authors do not discuss the fact that, because depletion of ARHGEF6 increases apoptosis, there are fewer neurons available for migration. This is important for the interpretation of the data. This point should be clarified.*

We appreciate this comment and believe that it is particularly relevant to the interpretation of the data shown in Figure 2F–G. We will clarify the limited interpretation of this specific analysis in the Results section. The altered directionality observed *in vivo*, together with evidence of impaired migratory behavior obtained through *in vitro* live imaging, supports the possibility that altered migratory dynamics contribute to the phenotype, although increased apoptosis and reduced neuronal output may also contribute.

> *(3) In Supplementary Figure S2, the authors describe the establishment of the ARHGEF6-KO human iPSC line and test the ability of these cells to undergo correct development, especially for the generation of neural progenitor cells. I was wondering why the authors do not present the data of both control and ARHGEF6-KO cells.*

We thank the reviewer for pointing this out. All staining reported in the organoids and assembloids in this paper shows that the WT ATCC-DYS0100 cell line, as well as the mutant, efficiently differentiates into neuronal tissue. The Supplementary Figure was intended to validate the impact of the mutation on the ability of the iPSC line to retain its differentiation capacity as a preliminary step before proceeding with organoid differentiation. We will integrate stainings for NPC markers on the WT line in the Supplementary Figure.

> *(4) At the molecular level, how ARHGEF6 depletion could affect neuronal survival is missing. In addition, as ARHGEF6 is a GEF for RAC1 and Cdc42 amongst other GEFs, I would have expected that the authors test how RAC1 activity (and Cdc42) is affected in ARHGEF6-depleted brains and in ARHGEF6-KO organoids. The measure of phalloidin staining and the anisotropy index are not really meaningful.*

We appreciate the thoughtful comment of the reviewer. Previous evidence already shows that *Arhgef6* loss reduces the activity of both GTPases and deregulates the expression of the cytoskeletal regulators Pak1–3, Limk1, and Cofilin in the mouse brain (Ramakers et al., 2012). Regarding organoids, we agree that direct RAC1/CDC42 activity measurements would have strengthened the molecular mechanism. We will revise the manuscript to avoid implying that our phalloidin-based measurements alone establish the underlying dysregulated molecular pathway.

> *(5) The authors show that ARHGEF6-KO forebrain organoids were markedly smaller compared to their isogenic controls, and their study suggests that ARHGEF6 expression impacts progenitor maintenance and neurogenesis. Despite representing only a minority of the total neuronal population, I was wondering whether ARHGEF6-KO mice present brain morphology defects such as microcephaly.*

We appreciate the comment. We did not perform a morphometric analysis for microcephaly in the present study. We will add this limitation to the Discussion and note that gross brain morphology changes were not reported in the previously published *ARHGEF6*-KO mouse characterization (Ramakers et al., 2012). We will also clarify that the smaller organoid phenotype may reflect developmental defects that may reflect developmental defects that are not fully compensated in a reductionist *in vitro* model and therefore do not necessarily imply overt microcephaly *in vivo*.

References

Allen Institute for Brain Science. Allen Mouse Brain Atlas: Arhgef6 ISH data. Available from: Allen Brain Map.

Birey, F., Andersen, J., Makinson, C. D., Islam, S., Wei, W., Huber, N., Fan, H. C., Metzler, K. R. C., Panagiotakos, G., Thom, N., O'Rourke, N. A., Steinmetz, L. M., Bernstein, J. A., Hallmayer, J., Huguenard, J. R., & Pașca, S. P. (2017). Assembly of functionally integrated human forebrain spheroids. Nature, 545(7652), 54–59. *https://doi.org/10.1038/nature22330*

Liaci, C., Camera, M., Zamboni, V., Sarò, G., Ammoni, A., Parmigiani, E., Ponzoni, L., Hidisoglu, E., Chiantia, G., Marcantoni, A., Giustetto, M., Tomagra, G., Carabelli, V., Torelli, F., Sala, M., Yanagawa, Y., Obata, K., Hirsch, E., & Merlo, G. R. (2022). Loss of ARHGAP15 affects the directional control of migrating interneurons in the embryonic cortex and increases susceptibility to epilepsy. Frontiers in Cell and Developmental Biology, 10, 875468. *https://doi.org/10.3389/fcell.2022.875468*

Nodé-Langlois, R., Muller, D., & Boda, B. (2006). Sequential implication of the mental retardation proteins ARHGEF6 and PAK3 in spine morphogenesis. Journal of Cell Science, 119(23), 4986–4993. *https://doi.org/10.1242/jcs.03273*

Pelkey, K. A., Chittajallu, R., Craig, M. T., Tricoire, L., Wester, J. C., & McBain, C. J. (2017). Hippocampal GABAergic inhibitory interneurons. Physiological Reviews, 97(4), 1619–1747. *https://doi.org/10.1152/physrev.00007.2017*

Ramakers, G. J. A., Wolfer, D., Rosenberger, G., Kuchenbecker, K., Kreienkamp, H.-J., Prange-Kiel, J., Rune, G., Richter, K., Langnaese, K., Masneuf, S., Bösl, M. R., Fischer, K.-D., Krugers, H. J., Lipp, H.-P., van Galen, E., & Kutsche, K. (2012). Dysregulation of Rho GTPases in the αPix/Arhgef6 mouse model of X-linked intellectual disability is paralleled by impaired structural and synaptic plasticity and cognitive deficits. Human Molecular Genetics, 21(2), 268–286. *https://doi.org/10.1093/hmg/ddr457*

Sloan, S. A., Andersen, J., Pașca, A. M., Birey, F., & Pașca, S. P. (2018). Generation and assembly of human brain region-specific three-dimensional cultures. Nature Protocols, 13(9), 2062–2085. *https://doi.org/10.1038/s41596-018-0032-7*

Yao, Z., Nguyen, T. N., van Velthoven, C. T. J., Goldy, J., Sedeno-Cortes, A. E., Baftizadeh, F., Bertagnolli, D., Casper, T., Chiang, M., Crichton, K., Ding, S.-L., Fong, O., Garren, E., Glandon, A., Gouwens, N. W., Gray, J., Graybuck, L. T., Hawrylycz, M. J., Hirschstein, D., … Zeng, H. (2021). A taxonomy of transcriptomic cell types across the isocortex and hippocampal formation. Cell, 184(12), 3222–3241.e26. *https://doi.org/10.1016/j.cell.2021.04.021*

https://doi.org/10.7554/eLife.111288.1.sa0